CORNEAL WOUND HEALING AFTER PHOTOREFRACTIVE KERATECTOMY: A 3-YEAR CONFOCAL MICROSCOPY STUDY

BY *Jay C. Erie MD*

ABSTRACT

Purpose: To perform a sequential quantitative analysis of corneal wound healing after photorefractive keratectomy (PRK) by using confocal microscopy in vivo.

Methods: In a prospective, nonrandomized, comparative trial performed in an institutional setting, 24 eyes of 14 patients received PRK to correct refractive errors between −1.25 and −5.75 D. Central corneas were examined preoperatively and at 1 day, 5 days, and 1, 3, 6, 12, 24, and 36 months after PRK by using confocal microscopy. A masked observer randomly examined 3 to 6 confocal scans per eye per visit to determine epithelial and stromal thickness, keratocyte density in 5 anterior-posterior stromal layers, corneal nerve density in the subbasal region and the stroma, and corneal light backscattering (corneal haze).

Results: Epithelial thickness increased 21% (*P*<.001) by 12 months after PRK and thereafter remained unchanged to 36 months after PRK. There was no change in stromal thickness between 1 and 36 months after PRK (*P* = .35). The dense keratocyte population in the preoperative anterior 10% of the stroma (32,380 ± 5,848 cells/mm^3) that was partially or completely removed during photoablation was not reconstituted at 36 months in the anterior 10% of the post-PRK stroma (17,720 ± 4,308 cells/mm^3, *P*<.001). Subbasal nerve fiber bundle density was decreased 60% at 12 months after PRK (*P*<.001) before returning to densities at 24 and 36 months after PRK that were not significantly different from preoperative values (*P* = 1.0). Activated keratocytes and corneal haze peaked at 3 months after PRK.

Conclusions: Wounding of the cornea by PRK alters the normal structure, cellularity, and innervation of the cornea for up to 36 months.

Trans Am Ophthalmol Soc 2003;101:287-328

INTRODUCTION

The reactions of the human cornea to surgical intervention have long interested ophthalmologists and have been the subject of several theses for the American Ophthalmological Society.[1-3] Photorefractive keratectomy (PRK), developed by Trokel and colleagues in 1983,[4] is a surgical procedure that uses the excimer laser to precisely photoablate graded amounts of anterior corneal stroma to induce a permanent and predictable change in corneal refraction.

The optics of the confocal microscope allow for noninvasive observation of cellular details, nerves, scar tissue, and keratocytes in unstained, living human corneas. This instrument provides *en face* optical sections of the cornea in vivo, in real time, and at magnifications sufficient to allow examination of cellular detail.

Additionally, examinations may be performed over time to allow observation of important cell-mediated processes such as wound healing. The availability of clinical confocal microscopy provides an opportunity to study how the human cornea may change after myopic PRK.

The goal of this study is to use confocal microscopy to study the human corneal wound healing response after myopic PRK with respect to changes in epithelial and stromal thickness, keratocyte morphology and density, corneal nerve morphology and density, and the development of corneal haze. Additionally, this work reviews the history and development of the confocal microscope and reviews the current knowledge of the corneal wound healing response to PRK, as related to the design and execution of the current prospective interventional study.

FOUNDATIONS OF THE CLINICAL CONFOCAL MICROSCOPE
Historical Perspectives
Hans Goldmann (1899-1991), best known in ophthalmology for developing and refining the slit-lamp microscope, the 3-mirror goniolens, and the applanation tonometer, published the first description of the clinical confocal

microscope in 1940.[5] Using a tandem scanning *slit* confocal microscope, Goldmann photographed the animal cornea ex vivo. Despite Goldmann's earlier description, most historians credit the invention of the confocal microscope to Professor Marvin Minsky, who published his idea as a patent in 1957 (Appendix 1).[6,7] Minsky, the son of an ophthalmologist, invented the scanning *point* confocal microscope while a Junior Fellow in the Harvard Society of Fellows. He developed the scanning point confocal microscope to "solve the problem of scattered light" while studying brain neural tissue. Using single pinhole field apertures, Minsky successfully blocked scattered light from out-of-focus parts of the specimen from reaching the final image. Minsky viewed the first confocal images of solid unstained tissues in real time on a military surplus radarscope. It was fortunate for Minsky that his brother-in-law, Morton Amster, not only liked the instrument but was also a patent attorney or the confocal microscope might never have been documented, as was the case with Minsky's earlier inventions of the micromanipulator and robot arm.[6]

In 1967, Mojmir Petran, a Professor of Biophysics at Charles University of Prague at Plzen, Czechoslovakia, along with Milan Hadravsky, developed a real-time tandem *point* scanning confocal microscope derived from a spinning Nipkow disk (Appendix 2).[8-10] Initial confocal images were of unstained tissue blocks of brain, ganglion cells, and animal corneas.[11,12] These observations were not repeated in the eye until 1986, when Lemp and colleagues[13] at Georgetown University, using the Petran tandem scanning Nipkow disk confocal microscope, observed the ex vivo cornea. Lemp subsequently arranged to have a Petran confocal microscope mounted on a headrest and applied it to observations of the in vivo human cornea. Lemp working with Jester and Cavanagh produced an elegant series of confocal studies on the rabbit eye and the in vivo human cornea by using digital image acquisition.[14-17] Subsequently, a clinical confocal microscope based on the Nipkow disk with an intensified video camera as a detector was developed by the Tandem Scanning Corporation, Inc.[17] This instrument contained an internal focusing lens that used a design first proposed by Masters,[18] which varied the depth of focus while the objective was held stationary on the surface of the cornea. This particular modification allowed accurate z-depth reproducibility. Later, Mayo Clinic investigators modified the instrument's joystick to simplify scanning and allow the examination to be completed by one technician (Figure 1).[19]

While Petran was developing the tandem *point* scanning confocal microscope, another group of investigators, an intellectual branch from Hans Goldman, was further modifying the scanning *slit* confocal microscope. In 1969,

Svishchev, in Moscow, designed and constructed a real-time scanning slit confocal microscope based on stationary slits and accomplished by an oscillating 2-sided mirror (bilateral scanning).[20,21] Simultaneously and independently, Baer patented a scanning slit confocal microscope that used movable slits (Appendix 3).[22,23] In 1974, Maurice enhanced resolution and contrast by narrowing the slit beam and reducing the volume of scattered light to obtain high-resolution, high-contrast images of the corneal epithelium and endothelium, stromal keratocytes, and Descemet's membrane.[24] In 1980, an improvement to the scanning slit specular microscope was designed by Koester and colleagues,[25] who used a scanning mirror system to move the slit over the tissue rather than the tissue over the slit. Later, based on Svishchev's design, a 2-dimensional, real-time, scanning slit confocal microscope was developed by Thaer and colleagues[26] and Masters and Thaer[27,28] for imaging the in vivo human cornea.

Optical Principles of the Confocal Microscope
The clinical confocal microscope was developed to optically section living human tissue. A confocal microscope illuminates *en face* optical sections of a thick translucent object, such as the cornea, with a focused spot of light by using a single microscope objective. The single objective is typically used for point illumination of the object and to simultaneously image the point of illumination on the aperture of the light detector (Appendices 1 through 3). For descriptive purposes, this is illustrated in Figure 2, in which two separate microscopes are placed on opposite sides of the cornea. A point source of light through aperture A1 is focused by lens L1 to an illuminated point in

FIGURE 1
The Tandem Scanning Nipkow disk-based confocal microscope (Tandem Scanning, Reston, Va). The objective lens is controlled from a computer joystick, custom-mounted onto the mechanical joystick of the microscope. Video imaging is provided by the VE-1000 SIT low-light camera (DAGE-MTI Inc) through a computer workstation (INDY, Silicon Graphics Inc).
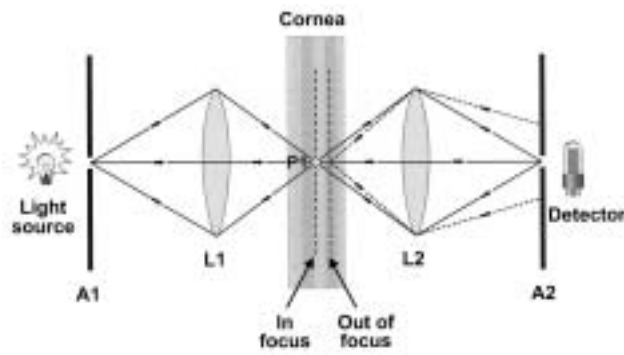
FIGURE 2

Principle of confocal microscopy. When the cornea is simultaneously in the focal plane of the illuminating light source and the detector, then both aperture A1 and A2 are cofocused (confocal) on the same point in the focal plane (P1). The resultant reflected light is focused on the pinhole and imaged by the detector (solid line). When the cornea is out of the focal plane, the defocused scattered light is spread out at aperture A2 and only a small amount of light is imaged by the detector (dashed line).

the focal plane of interest. The second lens, L2, is positioned so its focus is *coincident* with the same point of illumination. The second aperture, A2, is positioned so that the image of the illuminated spot formed by lens L2 is focused at aperture A2. Therefore, both the aperture A1 and the aperture A2 are *cofocused* (confocal) on the same point in the focal plane. Thus, the origin of the word confocal.

The confocal microscope discriminates against out-of-focus light that is not in the focal plane. Although the point of light imaged by lens L1 onto the thick cornea will focus light as a spot in the focal plane, there also will be light of lower intensity in the double cone on both sides of the focal plane. This out-of-focus scattered light is collected by lens L2, but the light is dispersed at aperture A2. Only a small amount of out-of-focus light enters aperture A2. As a result, the detector at A2 only detects a small amount of light from the out-of-focus planes (Figure 2).

The confocal microscope does not form an image of a single point within the object, but forms a 2-dimensional image. To form a 2-dimensional image it is necessary for the confocal microscope to scan the illumination spot over the area of the specimen. Minsky described in his patent two methods of point scanning: (1) stage scanning and (2) beam scanning.[7] Stage scanning requires the cornea to be moved across a stationary beam of light. In contrast, in beam scanning the illumination light is scanned across the stationary cornea. Beam scanning is used in modern clinical confocal microscopes.

Advantages of the Confocal Microscope
Two important imaging characteristics of the confocal microscope are (1) enhanced transverse resolution (x and

y coordinates in the plane of the specimen) and (2) enhanced axial resolution (z coordinate, which is orthogonal to the plane of the specimen), compared to a nonconfocal microscope that uses the same wavelength and the same microscope objective.[29] Resolution is 40% better in a confocal microscope than in a conventional microscope.[30] Improved transverse resolution permits higher resolution in the plane of the specimen. Improved axial resolution permits improved optical sectioning of thick specimens and their 3-dimensional reconstruction. These are important imaging advantages of the confocal microscope.

Clinically, the confocal microscope forms a new paradigm for visualization of living cells and tissue of the human cornea. This instrument provides an *en face* optical section of the cornea in vivo that is parallel to the corneal surface. All layers of the cornea can be imaged by changing the z-position of the objective. All examinations are in real time (image acquisition is at video rates). Magnification is sufficient to allow observation of cellular detail. Examinations can be performed over time to allow observation of wound healing. Finally, specimens in vivo can be viewed with the eye or an electronic detector.[29]

Limitations of the Confocal Microscope
The transverse and axial resolution in a confocal microscope depends on the wavelength of light and the numerical aperture of the microscope objective.[31] The tandem scanning confocal microscope uses short wavelengths of light and high numerical apertures. Shorter wavelengths of light yield greater resolution and are advantageous in imaging weakly scattering structures. However, in highly scattering structures, such as corneal scar tissue, shorter wavelengths increase light scatter and decrease penetration of light.[32] Similarly, microscope objectives with high numerical apertures yield greater resolution but consequently also (1) restrict the field of view on the specimen so that only a small area can be viewed and (2) restrict the free working distance of the microscope objective, thereby reducing the distance that the microscope can focus into the specimen from the surface.

Confocal microscopy of the living human cornea has two additional limitations. First, the cornea is a weakly reflecting specimen with low inherent contrast, resulting in a video image with reduced image quality. Second, the cornea is a moving object necessitating high scanning speeds. Eye movement can cause lateral and anterior-posterior motion blur. These physical limitations and other requirements must be taken into account in the design of a confocal microscope to observe the living human cornea. Each design of the following confocal microscopes is a trade-off and an optimization of design parameters.

Types of Confocal Microscopes

Tandem Scanning Nipkow Disk-based Confocal Microscope. The tandem scanning confocal microscope—utilized in the current study—uses the point scanning system developed by Minsky, Petran, and others (Figures 1 and 2). In this microscope, sets of conjugate pinholes (20 to 60 μm in diameter) are arranged in several sets of Archimedes spirals. Each pinhole on one side of the disk has an equivalent and conjugate pinhole on the other side of the disk. The illumination light passes through a set of pinholes (approximately 100) and is imaged by the microscope objective to form a diffraction-limited spot on the cornea. The reflected light from the cornea passes through a conjugate set (approximately 100) of pinholes on the other side of the disk and is recorded by the video camera. Both the illumination light and the reflected light are scanned in parallel ("in tandem") over the cornea to generate a 2-dimensional image of the focal plane by the spinning Nipkow disk. That is why this particular microscope is called a tandem scanning reflected-light microscope.[29]

The advantage of the tandem scanning confocal microscope is the exceptional transverse and axial resolution of the *point* scanning system. The disadvantage of this system is that the illumination is bright. Because the ratio of the area of the pinholes to the area of the disk is usually about 1%, only a small fraction of the illumination reaches the cornea. The cornea has low reflectivity, and of the small amount of light that is reflected from the cornea, only about 1% of this light passes through the disk from the microscope objective to the detector. Consequently, bright illumination like a xenon or mercury arc lamp is usually required and may cause patient discomfort.

One-Sided Nipkow Disk Confocal Microscope. In this confocal microscope design, the set of pinholes on the same side of the Nipkow disk is used for both illumination and detection.[33,34] An advantage of the one-sided Nipkow disk confocal microscope is a simpler optical design than the tandem scanning Nipkow disk confocal microscope. A disadvantage is that it is not easy to correct for chromatic aberrations because the illumination and reflected light follow the same optical path.[29]

Scanning Slit Confocal Microscope. An alternative approach to *point* scanning, as exemplified by the tandem scanning Nipkow disk confocal microscope, is to use a *slit* of illumination that is scanned over the back focal plane of the microscope objective. Slit scanning confocal microscopes, as developed by Goldman, Thaer, and others, have a much higher light throughput than confocal microscopes based on the Nipkow disk. This confers two advantages. First, the illumination on the patient's eye is much less and allows for longer scanning times and less patient discomfort. Second, it is possible to image low reflecting tissue and visualize the low reflecting layer of wing cells and basal cells in the epithelium. Only one group has used the pinhole-based confocal microscope successfully to image normal basal epithelial cells.[35]

The disadvantages of a slit scanning design can be significant. First, it has lower transverse and axial resolution than the pinhole-based confocal microscopes.[29] Second, in the currently available slit scanning systems there is no direct contact between the objective lens and the cornea; rather, immersion contact is made through a viscous gel on the tip of the lens, resulting in a large and variable working distance. In addition, current systems do not use an internal focusing lens. As a result, the microscope objective is not stationary at the corneal surface during scanning and does not allow an accurate or a repeatable determination of depth of the optical section inside the stroma or of overall corneal thickness.[36] Therefore, quantification per volume measurements is not justified.

Clinical Examination of the Human Cornea With the Confocal Microscope

Normal Cornea. The unique optical properties of the cornea are consistent with its morphology.[27,29,36,37] Consequently, the confocal microscope provides noninvasive observation of cellular details in unstained, living human corneas. In contrast, histologic studies are invasive, induce potential artifacts during processing, and cannot be used to study the cornea longitudinally or in vivo. Also, standard histologic sections give a sagittal view of the cornea, rather than the en face view (orthogonal to the thickness of the cornea) that is provided by the confocal microscope.

Epithelium. The early work by Calmettes an colleagues,[38] Ehlers,[39] and Wolff[40] measured epithelial thickness in humans by examining histologic specimens and found it to vary from 30 to 100 μm. Processing artifact makes interpretation of the data problematic. Reinstein and colleagues[41,42] used high-frequency ultrasound to document an epithelial thickness of 41 to 54 μm in conscious humans. The measurement of epithelial thickness by using the tandem scanning confocal microscopy in vivo is comparable to Reinstein and colleagues' measurements.[43-47]

In confocal microscopy, the anterior epithelial surface is defined by the highly visible superficial cells, which are about 4 μm thick (Figure 3A). Multicornered superficial cells show high and low reflectivity resembling the dark and bright cells of the epithelial surface seen in scanning electron microscopy.[29] Wing and basal cells have the lowest reflectivity of all cells in the cornea. Basal cells are

more easily detected by scanning slit confocal microscopy than tandem scanning confocal microscopy.[2,27] Basal cell density has been estimated at 5,600 to 6,200 cells/mm^{2} when a scanning slit confocal microscope is used.[36,48] The posterior border of the epithelium is defined by the subbasal nerve plexus, which is located in the basal aspect of the basal epithelial cells (Figure 3B).[49,50]

Bowman's Layer. Bowman's layer is 12 to 16 μm thick when measured by confocal microscopy.[41,43-45] This layer can be detected on the basis of its nonreflectivity, which contrasts with the visible overlying subbasal nerve plexus and the underlying first keratocyte layer.[43]

Stroma. In the healthy human cornea, quiescent keratocyte nuclei are seen as bright objects. The cell bodies, the keratocyte processes, and the stromal collagen and ground substance are not visible.[36,44,51-54] The shape and spatial arrangement of keratocyte nuclei in confocal images of the corneal stroma are specific for their location.[44,53,54-58] The most anterior keratocyte nuclei are smaller, more numerous, and have a characteristic morphology with multiangulated nuclei (Figure 3C). The middle and posterior stromal keratocyte nuclei are less numerous and round to oval with occasional indentations (Figure 3D). An additional narrow layer (1 to 2 consecutive confocal images) immediately subjacent to Descemet's membrane consists of numerous posterior keratocytes that have a more elongated appearance.[44,53,55,58] Between the layers of the stromal collagen, branching nerve fiber bundles or trunks of variable size are seen with high reflectivity (Figure 3E).[59,60]

Descemet's Layer And Endothelium. Similar to Bowman's layer, Descemet's membrane is poorly reflective and serves to contrast the most posterior keratocyte layer and the corneal endothelium. The endothelium is clearly visible in normal human corneas (Figure 3F).[43,44]

In Vivo Capabilities of the Confocal Microscope

Thickness Estimates of the Cornea and its Sublayer. An accurate and reproducible thickness measurement of the cornea and its sublayers is important for the sequential examinations used in studying corneal wound healing in vivo. The mean measured thickness of the cornea by various instruments and techniques has not been consistent. The mean corneal thickness measured by various clinical ultrasonic pachometers ranges from 512 to 638 μm, depending on the design and particular manufacturer of the instrument.[61-65] The variability of ultrasonic pachometry has been reviewed by Waring.[66] The mean corneal thickness measured by optical pachometers, such as the Haag-Streit with subjective endpoints, varies from 490 to 581 μm in normal subjects.[67,68] Interferometric methods indicate a mean thickness of 524 to 536 μm.[69,70] Objective systems based on the slit lamp[71] and a custom high-

frequency ultrasonic pachometer[41] indicated a mean corneal thickness of about 515 μm. Estimates of the mean corneal thickness in a normal population may vary with the design or manufacturer of the pachometer.

An ideal method of measuring depths in the cornea would allow the investigator to actually see the structures at the depth being measured, such as the surface of the epithelium, the subbasal nerve plexus, the first keratocyte layer, or the endothelium, and associate these visible features with depth. Tandem scanning confocal microscopy has this ability.[29]

Tandem scanning confocal microscopy allows one to examine the cornea in vivo by optically advancing a thin (9 μm) focal plane at a constant speed through the cornea while recording video images.[72] Depth of visible structures in the video images can be determined from the sequential video-frame number relative to a fixed reference (epithelial surface).[44,47,58,72] Depth can be specified to within the distance the focal plane travels during one frame, approximately 2.6 μm with a tandem scanning confocal microscope.[44,58,72] Some investigators have improved spatial resolution by using one half of each interlaced video frame to determine the location of objects.[43] Absolute depth can be determined by knowing the relationship between the scan speed of the focal plane and the video-frame rate.[44,58] Consequently, investigators have developed quantitative techniques using digital image analysis of continuous, high-speed confocal z-scans to obtain precise in vivo corneal thickness measurements and sublayer thickness measurements of the epithelium, Bowman's layer, and stroma.[43-45,47,73]

Recently, Nau and colleagues[74] designed a method of calibrating and correcting distance measured by tandem scanning confocal microscopy for the nonlinearity between video-frame number and actual depth. Their method also corrected for error induced by refraction at the surface of the cornea and for the curvature of the corneal surface. With their technique, the mean measured thickness of polymethylmethacrylate contact lenses was not significantly different from the thickness measured by using a micrometer (difference = 0.01 μm ± 3.5 μm). Applying their method clinically to visualize epithelial and endothelial surfaces in vivo, Nau and colleagues[74] determined the mean human corneal thickness to be 525 ± 28 μm.

The primary source of random error when using tandem scanning confocal microscopy to measure corneal thickness in alert humans is corneal motion during the confocal measurement.[29,75] Scanning in both directions (anterior to posterior and posterior to anterior) and accepting only measurements that are within ± 10 μm minimizes corneal motion artifact. With this scanning technique, the precision (± SD) of confocal microscopy in
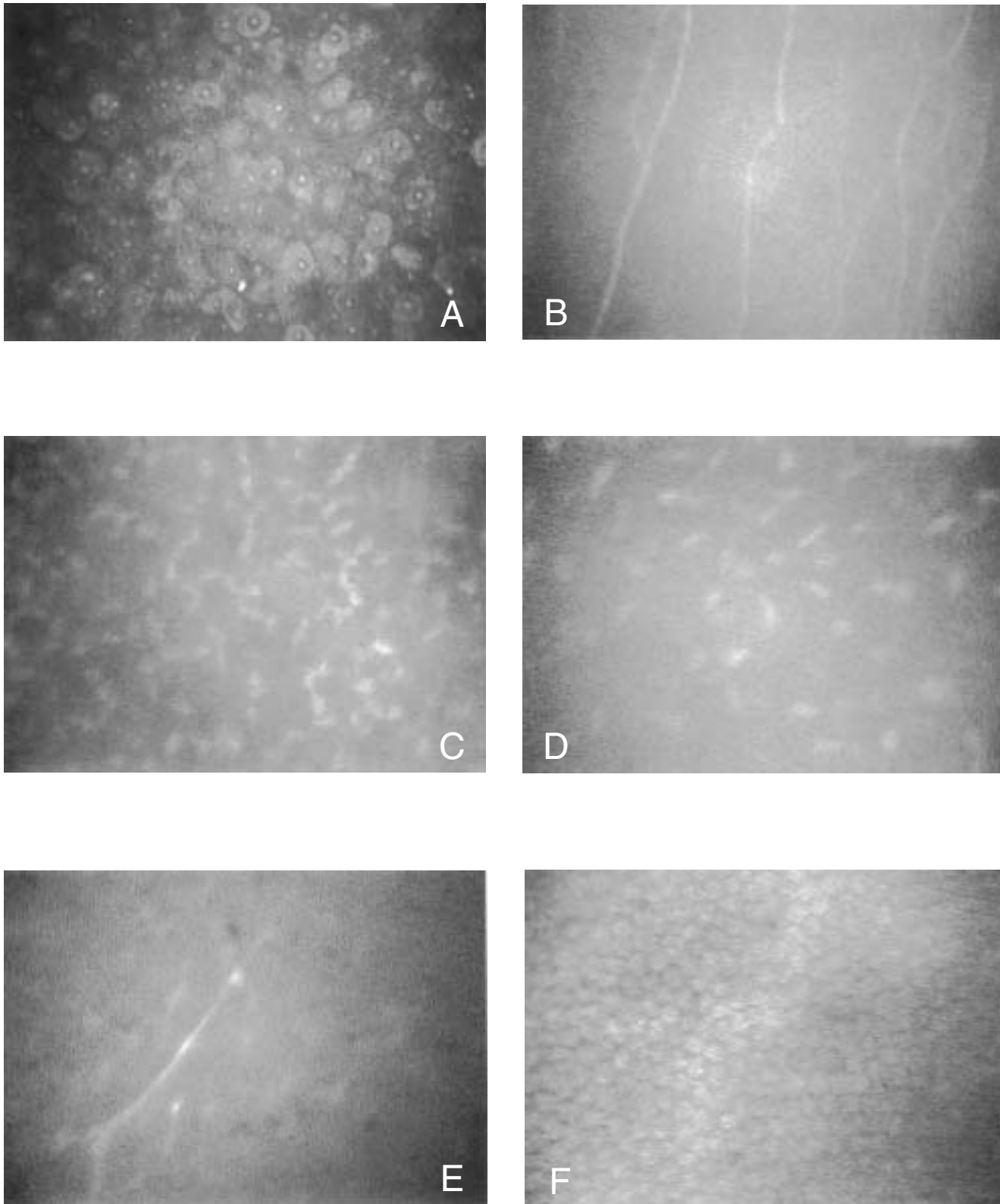
FIGURE 3

Confocal section of a normal cornea. A, The surface epithelial cells. Dark and light cells are visible with dark nuclei. B, Parallel and vertical orientation of the central subbasal nerve fiber bundles presenting as long branching linear structures located at the basal aspect of the epithelial cell layer. C, Small, numerous anterior keratocyte nuclei with a characteristic multiangulated border. D, The cell nuclei of midstroma keratocytes have a round to oval shape and are the predominant type throughout most of the stroma. E, A nerve fiber bundle, which is highly reflective, is seen located parallel to the tissue layer. F, The endothelial monolayer.

measuring corneal thickness is comparable to ultrasonic pachometry.[74]

Assessment of Keratocyte Density. In 1993 Cavanagh and colleagues[76] published confocal microscopy findings of a normal cornea in a 52-year-old man. Subjectively, there appeared to be large numbers of keratocytes present in the anterior stroma compared with the middle and posterior stroma. Later, in vitro studies of human eyes that used light and electron microscopy,[56] vital dyes,[55] and DNA distribution[77] found a 30% decrease in cell density over the anterior-posterior stromal thickness. Subsequent confocal microscopy studies of animal[73,79,80] and human[36,44,52,53] corneas in vivo quantitatively confirmed the original confocal observations of Cavanagh and colleagues[76] of a higher number of keratocytes in the anterior stroma than in the posterior stroma. Keratocyte density is greatest in the anterior stroma 50 to 100 µm immediately posterior to Bowman's layer. Within this anterior stroma, cell density is greatest in the most anterior countable confocal image.[44,75] With aging, the full-thickness keratocyte density decreases 0.3% per year, and this decline in keratocyte density parallels the age-associated decline in endothelial cell density.[44,78,81]

Patel and colleagues [44,45] have described quantitative methods for measuring keratocyte density by using confocal microscopy in human and rabbit corneas in vivo and have validated these measurements by comparing keratocyte density measured by confocal microscopy with density estimated from histologic sections of the same tissues. As a result, confocal microscopy in vivo has been used to determine corneal keratocyte density in normal corneas,[36,44,52,53] in contact lens wearers,[82] in keratoconus,[73] in Fuchs' dystophy,[83] after penetrating keratoplasty,[81] after myopic LASIK,[84] and after myopic PRK.[54,85]

Assessment of Keratocyte Morphology. Poole and colleagues[55] using vital dyes and later Hahnel and colleagues[80] using confocal laser scanning microscopy in vitro identified three morphologically different keratocyte subpopulations. Similarly, confocal microscopy studies have described three morphologic types of keratocyte nuclei throughout the normal cornea.[29,38,44,51,53]

In confocal images of the human cornea, the quiescent or resting keratocyte nucleus appears as a bright oval- to bean-shaped object against a dark background. Cellular processes are not evident.[36,44,51-54] The proliferating, activated repair-fibrocyte or myofibroblast has a prominent rough endoplasmic reticulum that is not seen in the quiescent keratocyte, implying active protein synthesis.[86,87] Consequently, the activated keratocyte has greater corneal light backscattering than the quiescent keratocyte during confocal microscopy. As a result, activated keratocytes have a large, brightly reflective appearance in confocal images, and their cytoplasmic processes

are often visible.[47,81,84,85,88] The appearance and disappearance of activated keratocytes over time has been followed by using the confocal microscope.[47,51,54,84,85,88,89]

Assessment of Corneal Nerve Morphology and Density. Early studies of corneal nerve organization were derived from light and electron microscopy of animal and human corneas. These studies, using different staining and fixation techniques and varied methods of analysis, have provided information on the morphology, ultrastructural organization, and innervation density of corneal nerves.[49,50,90,91] Most histologic studies were performed in eyes postmortem. Muller and collegues,[49] using electron microscopy, demonstrated that human corneal nerves degenerate within 13.5 hours after death, which creates difficulties for accurate structural analysis of human corneal nerves. In addition, the values given for nerve density in histologic studies are influenced strongly by the section, fixation, and staining procedures and the form of image analysis used.[55]

The availability of confocal microscopy for repeated, noninvasive imaging of the human cornea in vivo is therefore beneficial for analysis of corneal nerves. Nerve fiber bundles are easy to identify by confocal microscopy (Figures 3B and 3F). They appear as bright, well-defined, linear structures with homogeneous hyperreflectivity.[29,55,81,92-94] Chiou and colleagues[92] identified many linear features by clinical confocal microscopy, including vessels, lattice dystrophy, posterior polymorphous dystrophy, and fungal keratitis, although the only linear structures in normal corneas consisted of nerves. Nerve fiber bundles contain several nerve fibers.[50] Individual nerve fibers cannot be seen with the clinical confocal microscope.[29,59,60,95] Therefore, confocal microscopy studies have taken the approach used by Muller and colleagues[49,50] and used the phrase "nerve fiber bundles" to emphasize that individual nerve fibers are not visible.

Recent studies suggest a high concordance between the observations of corneal nerves made by confocal microscopy in vivo[59,60] and the information obtained in previous histologic studies.[49,50,90,96-99] Confocal microscopy has been shown to be helpful in describing the morphology of nerves in normal corneas,[59,60] in corneas of diabetic patients with and without neuropathy,[100] after LASIK,[93,101-103] and after PRK.[95,104] The quantification of corneal nerve density, however, has been attempted in only normal corneas[59,60] and after LASIK.[101]

Confocal microscopy has limitations when used to assess corneal nerve fiber bundles. First, because of the narrow field of view, a false-negative result may be obtained. Second, the alignment of the microscope tip must be adjusted parallel to the surface of the cornea; otherwise, the images of nerve fiber bundles are oblique, and long nerves may be falsely considered short. Third,

individual nerve fibers and the intraepithelial axon terminals oriented vertically from the subbasal nerve fiber bundles cannot be visualized with a tandem scanning confocal microscope. Finally, in post-PRK eyes, the absence of a dark Bowman's membrane and the presence of a highly reflective haze may make visualization of the corneal nerve fiber bundles difficult.[59,95,104]

Assessment of Corneal Haze. The development of optical disturbances in corneal transparency is termed "haze." A few objective clinical haze assessment techniques have been reported: high-frequency ultrasound,[105] Scheimpflug photography,[106] and light-scattering measurements.[107-109] The assessment of corneal haze after PRK, however, primarily depends on slit-lamp biomicroscopy, which generally has a low reproducibility and high interobserver variability.

The confocal microscope provides for a noninvasive, quantitative measurement of corneal light backscattering (haze).[47,82,85,110-113] In previous studies in humans and rabbits, a significant correlation was found between the clinical haze grading and the objective confocal microscopy haze value.[47,88] Furthermore, the measurement of confocal microscopy haze was more sensitive than slit-lamp biomicroscopy and allowed identification of subtle (subclinical) alterations in corneal transparency in corneas that were graded as clear by slit-lamp examination.[47] Confocal microscopy haze values have been shown to peak at 3 months after PRK,[110,111] to be significantly correlated with the depth of excimer ablation,[47,110] and not to be correlated with the amount of refractive regression,[110] which is consistent with the clinical observations of others.[114,115]

PHOTOREFRACTIVE KERATECTOMY

Previously, researchers approached epithelial and stromal wound healing as separate events. Recently, it has become increasingly clear that all corneal wounds—including those created by PRK—stimulate both an epithelial and a stromal healing response. Thus, the interaction between stromal and epithelial healing must be considered to fully understand corneal wound healing.

Epithelial Response
The epithelial covering of the ablated corneal surface after PRK is an early and important step in wound healing. Corneal epithelial wound repair is a multifaceted process that can be divided into three overlapping phases.[116] In the first phase, which lasts about 8 hours, the epithelial cells prepare to migrate onto the wound surface. The hemidesmosomal attachments between the basal cells and the basement membrane disappear from the wound edge.[117] Superficial cells are desquamated, leading to a thinner epithelium at the wound edge.[118] The cells

synthesize structural proteins, and actin filaments are assembled in the basal region of the migrating cells.[119] The formation of lamellipodia and filopodia marks the beginning of the second phase, or the migration of the epithelial cells onto the wound surface.[116] The actin filaments are considered to make the cells move.[119] This early movement is independent of cellular division.[120,121] In addition to migration, the cells also increase their volume to cover a large area. The reepithelialization of the cornea is usually accomplished in 2 to 4 days after PRK.[89,95,122,123] After wound closure, the epithelium consists of one to two cell layers. The cells are subsequently replaced by division and centripetal migration from a population of slow-cycling stem cells in the basal layer at the limbus.[124,125] Cytokines produced by underlying repair-fibrocytes, in part, regulate the proliferation, migration, and differentiation of the healing epithelium.[126] In the final phase, hemidesmosomes are permanently reformed and reassembly occurs, a process that requires weeks after PRK.[127,128]

Stromal Response
Stromal wound healing after PRK also occurs in phases and depends on a coordinated interaction between epithelial cells and keratocytes.[129] In the first phase, superficial keratocytes disappear in the area adjacent to the epithelial debridement. This observation was made first by Dohlman and colleagues[130] more than 30 years ago. In the years that followed, this same observation was made independently in various species.[131-134] In 1996, Wilson and colleagues[135] first reported that this disappearance of keratocytes was mediated by apoptosis. This type of cell death induces minimal local damage to surrounding cells and has been suggested to initiate the healing response.[136] Subsequently, several studies have suggested that injury-induced keratocyte apoptosis is mediated by the release of proapoptotic cytokines from the injured epithelium.[135,137] Cytokines that have been implicated include interleukin (IL)-1, Fas ligand, bone morphogenetic protein 2, bone morphogenetic protein 4, and tumor necrosis factor.[135,138-140] After epithelial injury, implicated cytokines are released. These cytokines bind to receptors on keratocytes immediately beneath the wounded epithelium and set in motion a complex cascade of epithelial and stromal wound healing events.

In the second phase of stromal wound repair, the remaining keratocytes surrounding the area of apoptotic loss begin to undergo proliferation to repopulate the wound area.[141] In rat corneas, proliferation occurs 24 to 48 hours after wounding.[142,143] As part of this second phase, these proliferating cells activate or transform into wound-repair keratocyte-derived cells or repair-fibrocytes.[144,145]

The first detectable changes are an increase in keratocyte size and an increase in the size and number of nucleoli, the organelle in which ribosome synthesis occurs.[85,86] The proliferation and migration of repair-fibrocytes is probably mediated by platelet-derived growth factor released from the epithelium.[146] The migrating repair-fibrocytes also may synthesize and deposit matrix components during this phase.[110,147] Over time, repair-fibrocytes gradually become more quiescent and take on a keratocyte appearance, although biochemically they continue to resemble fibrocytes.[86]

Much of the synthetic activity of the repair-fibrocyte at this point is involved with the production of the repair extracellular matrix (ECM), which has a composition different from that of the normal stroma.[148] ECM components that are not normally present in the central cornea include fibronectin, fibrin, tenascin, and chondroitin sulfate.[149,150] The ratio of collagen types synthesized by the repair-fibrocyte is different from the types found in the normal stromal ECM.[151] Recent reports suggest that fibronectin and chondroitin sulfate promote entry of migrating fibroblasts into the wound area.[152]

IL-1 and other cytokines also stimulate repair-fibrocytes to produce metalloproteinases, collagenases, and other enzymes that turn on new synthesis of enzymes that can degrade ECM.[153] The ECM of the repair tissue is remodeled progressively by continual synthesis, degradation, and resynthesis of collagens and other ECM components. Key growth factors regulating this response are hepatocyte growth factor and keratinocyte growth factor.[154,155] The receptors for these cytokines are expressed by the epithelium and are up-regulated in response to injury.[127]

The final phase involves contraction of the wound and appearance of new cell type: the myofibroblast. The myofibroblast, a reversible phenotype of the repair-fibrocyte, is characterized by the intracellular appearance of α-smooth muscle actin.[156,157] Wounds that were originally horizontal and removed basement membrane, such as those created by PRK, result in the generation of more myofibroblasts than wounds that do not penetrate basement membrane.[158] After PRK, the myofibroblast cells eventually disappear in weeks to months with minimal scarring.[141] It is unclear how myofibroblasts are eliminated from the stroma, but there is some evidence that late apoptosis may be involved.[159]

Keratocyte Density

The stromal keratocytes of the mammalian cornea originate from the second of three waves of neural crest–derived mesenchymal cells that enter the eye during its embryonic development.[86] Keratocytes are distributed throughout the human corneal stroma in a nonuniform pattern.[44,51,55,57] Keratocyte density is 40% higher in the anterior 10% of the stroma compared with the mean density of the remaining stromal layers.[44,51] PRK removes Bowman's layer and a variable amount of anterior stroma that contains a large number of keratocytes.

Rabbit studies after PRK indicate that anterior stromal keratocytes adjacent to the wound area disappear by apoptosis.[126,137,141,160,161] After cell loss, keratocytes rapidly repopulate the area to a much greater density than in the normal corneal stroma, before eventually returning to preoperative levels.[123,161-165]

Results of nonhuman primate histologic studies,[87,128,166-169] which show a high degree of similarity to those of human studies, also demonstrate an initial loss of anterior keratocytes after PRK, followed by an apparent increase in keratocytes (viewed in histologic sections but not quantified) in the anterior stroma that persists for 3 to 4 months after PRK.

Human histologic studies[170-173] suggest that anterior keratocytes respond to PRK in a manner similar to animal models. However, there are few human in vivo studies that have attempted to quantify keratocyte density after PRK.[51,54,85,173] Using confocal microscopy, Corbett and colleagues[85] found that the anterior keratocyte density increased 50% by 2 days after PRK, increased 100% by 1 month after PRK, and returned to preoperative density by 6 months after PRK. Frueh and colleagues[54] used confocal microscopy to show a 15% increase in anterior keratocyte density at 1 and 4 months after PRK, before it returned to preoperative densities by 1 year after PRK. Erie and colleagues[51] used confocal microscopy to demonstrate a 20% increase in keratocyte density 3 months after PRK. Increases in keratocyte density after PRK in humans are thought to occur by keratocyte migration and by keratocyte mitosis, which have been demonstrated in mice after epithelial scraping.[142,143]

Corneal Opacification: Haze and Scarring

A frequent consequence of excimer laser PRK is the development of variable degrees of optic disturbances in corneal transparency termed corneal haze.[3,87,114,115,128,169,174,175] In general, haze after PRK in humans is notably less than in animal studies, including nonhuman primates.[3] Haze often is mild and transient and disappears within the first year. However, visually debilitating haze may persist in approximately 5% of all PRK patients.[176,177] The term "scarring" has been reserved for grade 4 haze.[178] Investigators disagree on the benefit of a topical corticosteroid regimen in reducing haze after PRK.[175,178,179]

Researchers have attributed haze (backscattered light) after PRK to the putative changes in the stromal ECM and the highly reflective activated keratocytes.[85,110] Evidence of new ECM deposition after PRK has been

demonstrated in histologic[172,180-182] and confocal microscopy[76, 110] studies in humans. The composition of new subepithelial ECM after PRK includes glycosaminoglycans, fibronectin, laminin, type III collagen, keratin sulfate, and hyaluronic acid.[168,182] The altered composition of repair ECM and the disorganized manner of its deposition result in scattered light and contribute to subsequent haze. The new subepithelial interface after PRK also accumulates water that colocalizes with the hyaluronan.[183] The sharp demarcations of these zones create sharp shifts in refractive index in these areas, causing light scattering.

Haze has also been attributed to changes in individual activated keratocytes. Keratocytes form an interconnecting network that is essentially transparent to light passing through the cornea. Apparently this is because of high concentrations of specific intracellular protein molecules that affect the refractive index of the cells.[157] These cytosolic, water-soluble proteins, termed crystallins, appear to control the optical properties of individual keratocytes and have been shown to be altered after PRK in humans, consequently altering corneal clarity.[110]

Regeneration of Corneal Nerves
The human central cornea is densely innervated by nerve fibers of the ophthalmic division of the trigeminal nerve. Radially oriented thick stromal nerve bundles penetrate the limbus in the anterior and middle third of the stroma. The nerve bundles lose their myelin sheaths and divide dichotomously or trichotomously. Before penetration of Bowman's layer to enter the epithelium, the stromal nerve bundles bend at right angles and lose their Schwann cells. They bend again at right angles and are parallel to and between the basal cell layer and Bowman's layer to form the subbasal nerve plexus.[50, 90] This parallel organization seems to be specific for the human cornea.[50, 90,184] The subbasal nerve fiber bundles are oriented between 5 and 11 o'clock and 7 and 1 o'clock in the central cornea and are in an oblique or horizontal direction in the central-peripheral and peripheral cornea.[49,50,55,56] From these bundles, a regular meshwork of finer branches is oriented vertically, terminating as intraepithelial free nerve endings.

PRK photoablates and destroys the nerves of the subbasal plexus and the anterior stroma, leaving sharply cut nerve trunks at the base and margin of the wound. Rabbit studies after PRK have shown that corneal nerve regeneration is a biphasic process.[97,185,186] Rabbit data are thought to be applicable to humans because the sensory innervation of the rabbit and primate corneas is similar, and the sensory nerves of human and rabbit corneas show histochemical acetylcholinesterase reaction.[90,97] In the first phase of rabbit corneal nerve regeneration, the reinnervated subepithelial plexus is formed by fine neurites that originate from the cut peripheral subepithelial plexus and course centrally with the migrating epithelial cells.[91,97,185,186] Using histochemical techniques, Trabucchi and colleagues[187] showed that the newly regenerated subepithelial neurites appeared as early as 1 day after PRK in rabbits. Pallikaris and colleagues[188] made similar observations. Tervo and colleagues[97] demonstrated that regenerating neurites extended 1.5 to 2.0 mm from the wound margin at 6 weeks after PRK. By 3 months after PRK, a normal density of intraepithelial nerve terminals was achieved. Ishikawa and colleagues[189] demonstrated a transient increase in the density of intraepithelial nerves in the rabbit after PRK, which returned to normal density about 7 months after surgery.

The second phase of nerve regeneration in the rabbit is initiated by the degeneration of the wound-oriented neurites and the concomitant appearance of a second generation of stromal neurites that ultimately reestablish a new subepithelial plexus.[185,186] The new second-phase neurites originate from the transected stumps of stromal nerves at the wound base and margin and first appear at the cut nerve edge about 2 weeks postinjury in rabbits.[186] The regenerating stromal nerves reach the epithelium and contribute to the formation of a new subepithelial plexus at 6 months after PRK.[97,187] One year after PRK, the subepithelial nerves regain normal density and architecture, although the stromal nerve architecture is still abnormal.[97]

In humans, subbasal nerve fiber bundles have been described after PRK by using tandem scanning confocal microscopy in vivo,[48,54,85,95] although none of these studies attempted to quantify nerve density. These qualitative studies suggest that the degree of regeneration of the subbasal nerve plexus varies in humans after PRK.[95] Auran and colleagues[91] measured the velocity of nerve growth in the basal epithelial plexus in humans by means of a confocal microscope and found it to vary between 7 and 17 μm daily. Linna and Tervo[95] identified regenerating fine subbasal nerve fibers at 1 week post-PRK, whereas Frueh and colleagues[54] identified subbasal nerves in only 1 (6%) of 18 eyes 1 month post-PRK. Kauffmann and colleagues[103] and Corbett and colleagues[55] described partial or complete reinnervation at 8 to 12 months after PRK.

Stromal nerve fiber bundles in the normal human cornea have been quantified and found to be limited to the anterior 60% of the stroma.[50,59] Linna and Tervo[95] described a persistent abnormal morphology of regenerated anterior stromal nerves after PRK in humans and inferred a lower density up to 34 months postoperative. No other human studies have attempted to quantify stromal nerves after PRK.

METHODS

SUBJECTS

Twenty-four eyes of 14 subjects (3 men, 11 women) were enrolled prospectively in a nonrandomized fashion from July through October 1998. All participants were patients at the Mayo Clinic, Rochester, Minnesota. Mean subject age was 40 ± 7 years (range, 22-53 years) and the mean preoperative spheroequivalent refractive error was -3.73 ± 1.30 D (range, -1.25 to -5.75 D). All subjects were white. None of the 14 subjects had a history of anterior segment disease, ocular trauma or surgical procedures, diabetes mellitus, or the use of ocular medications. Systemic medications were permitted, unless they were known to affect the cornea or the anterior segment. Contact lens wear was discontinued 2 weeks (soft lenses) or 3 weeks (rigid gas permeable lenses) before the study. Corneas were examined by slit-lamp biomicroscopy to assess whether they were normal. Subjects were excluded if intraocular pressure was more than 22 mm Hg or asymmetric (difference between eyes of >3 mm Hg). During the eligibility examination, corneal thickness was measured by ultrasonic pachometry (Pachette; DGH Technology Inc, Exton, Pa), corneal topography was obtained (TMS-2, Tomey USA, Cambridge, Mass), and a manifest and cycloplegic refraction was performed. This study was approved by our institutional review board and adhered to the tenets of the Declaration of Helsinki. Informed consent was obtained from all subjects after explanation of the nature of and possible consequences of participation in the study.

PRK PROCEDURE AND POSTOPERATIVE REGIMEN

PRK for myopia or myopic astigmatism was performed by using the VISX Star laser (VISX, Santa Ana, Calif) with a wavelength of 193 nm, fixed pulse rate of 6 to 8 Hz, and radiant exposure of 160 mJ/cm². The epithelium was removed from a circular area with a 6.3 mm diameter by using the laser-scrape technique (43-μm epithelial ablation followed by manual scrape of the remaining epithelial cells with a blunt spatula). The ablation zone ranged from 6.0 x 6.0 mm for spherical corrections to 5.0×6.0 mm for astigmatic corrections. The mean planned ablation depth was 46 ± 18 μm (range, 13 to 90 μm). Emmetropia was attempted in all cases. Immediately after the ablation, the cornea was cooled for 30 seconds by irrigation with cold balanced salt solution.

After the PRK procedure, patients wore a bandage soft contact lens (SofLens 66, Bausch & Lomb Inc, Rochester, NY) until the cornea epithelialized (2 to 5 days). Topical medications consisted of preservative-free ketorolac tromethamine 0.5% (Acular PF, Allergan Inc, Irvine, Calif) for four doses over 2 days, ofloxacin 0.3% (Ocuflox, Allergan Inc) four times daily until epithelializa-

tion was complete, and fluorometholone 0.1% (FML, Allergan Inc) four times daily with taper over 3 months. Eyes were examined by confocal microscopy and by slit-lamp biomicroscopy before PRK and at 1 and 5 days and 1, 3, 6, 12, 24, and 36 months after PRK. At all visits between 1 and 36 months post-PRK, a manifest refraction was performed and the density of central corneal haze was graded by using the standardized clinical categories described by Fantes and colleagues.[87]

A bandage soft contact lens was already in place on all of the eyes at the 1-day examination. To protect against possible corneal abrasion, the bandage soft contact lens was placed for approximately 15 minutes on all of the eyes at the 5-day examination and on 3 eyes at the 1-month examination. A bandage contact lens was not used thereafter.

CONFOCAL MICROSCOPY IN VIVO

A Tandem Scanning Nipkow-based Confocal Microscope (Tandem Scanning, Reston, Va) was used to examine the central corneas in vivo, as described previously.[44,58] The microscope had a 24×, 0.6-numeric-aperture objective lens with a concave surface and a working distance of 0 to 1.5 mm. The position of the optical plane could be advanced or retracted by an internal lens without changing the position of the front surface of the objective. The objective lens was controlled from a computer joystick, custom-mounted onto the mechanical joystick of the microscope,[44,58] and connected to an encoder mike controller (Oriel 18011, Oriel Instruments, Stratford, Conn) through a computer workstation (INDY, Silicon Graphics Inc, Mountain View, Calif). Images were recorded by a low-light camera (VE-1000 SIT, DAGE-MTI Inc, Michigan City, Ind) and digitalized and stored directly into computer memory at 30 frames/second. With this objective and camera, each *en face* 2-dimensional image represented a coronal section (x-,y-axis) of 475 μm × 350 μm (area, 0.166 mm²) and a depth of field (z-axis thickness) of 9 μm. Each image was separated from the adjacent image by an average of 2.6 μm.[44,58]

Proparacaine hydrochloride 0.5% (Bausch & Lomb Pharmaceuticals, Inc, Tampa, Fla) was instilled into the eye to be examined. One drop of 2.5% hydroxypropyl methylcellulose (CIBA Vision Ophthalmics, Atlanta, Ga) optical coupling medium was placed on the tip of the objective lens. The objective was carefully aligned to the visual axis of the eye and manually advanced until the medium contacted the central cornea. The position of the objective was adjusted to provide an *en face* view of the central cornea to confirm correct alignment. The patient self-fixated on a bright target with the contralateral eye to minimize eye movements.

During the confocal examination, the optical section was advanced through the full-thickness cornea at a constant speed of approximately 78 μm/second. A series of confocal images (constituting one scan) was recorded in approximately 7 seconds as the optical section advanced from anterior to the epithelium to posterior to the endothelium (continuous through-focusing). The objective was withdrawn from the cornea after each scan. Four to eight scans without significant eye movement were recorded per visit. Images were acquired by setting the camera either in a fixed-gain mode, with a constant gain, voltage, and black level, or in automatic-gain mode, with these parameters automatically adjusted by the camera throughout image acquisition.

THICKNESS MEASUREMENTS

All scans were reviewed manually, and the scans with the least lateral ocular movement and with no obvious anterior-posterior movement of the objective relative to the cornea were selected for analysis. We generated an intensity profile of backscattered light from selected confocal images obtained by continuous through-focusing of the optical plane (Figure 4).[43,44,47,102,110,111] Images were acquired with the camera operating in its fixed gain mode. Intensity was estimated from the mean grayscale value in a 300×300 pixel area in the center of each image. Peaks in intensity corresponded to the superficial epithelium, the subbasal nerve plexus, the most anterior keratocytes, and the endothelium (Figure 4). The video image corresponding to each intensity peak was displayed, and the first focused video image of each corneal region was identified and used in the determination of thickness. In profiles generated from corneas after PRK, a peak corresponding to anterior stromal haze was often present, as confirmed by the presence of increased reflectivity of keratocyte nuclei and cell bodies in the corresponding video image. If intensity peaks were not evident in the light intensity profile or if peaks did not correspond to the appropriate region of the cornea, the first focused video image of each corneal region was identified and then used in the determination of thickness.

Corneal thickness was defined as the distance between the first focused image of the superficial epithelium and the endothelium. Epithelial thickness was the distance between the first focused image of the superficial epithelium and the subbasal nerve plexus.[50] The subbasal nerve plexus is not always present after PRK because it is destroyed by laser-scrape epithelial removal and the subsequent photoablation. Therefore, when subbasal nerves were not visible in images after PRK, we determined epithelial thickness as the distance between the first focused image of the superficial epithelium and the first focused image of anterior keratocytes.

Bowman's layer cannot be visualized in the preoperative cornea with a tandem scanning confocal microscope. The thickness of Bowman's layer, however, can be determined from the distance between the first focused image of the subbasal nerve plexus and the most anterior keratocytes. Stromal thickness was the distance between the first focused image of the most anterior keratocytes and the last focused image of the posterior keratocytes having a reflected light intensity similar to other images of the stroma but without images of endothelial cells, in an attempt to exclude Descemet's membrane.

An estimate of the stromal thickness destined to be ablated, or the actual photoablation depth, was obtained as the surgically induced stromal thinning (S_{thin}) between the pre-PRK (S_{pre}) and 1-month post-PRK (S_{post}) measured stromal thickness.

$$S_{thin} = S_{pre} - S_{post}$$

Stromal regrowth was defined as the change in stromal thickness between 1 and 36 months after PRK.

The stroma was subdivided by depth into 5 layers; 0% to 10% (anterior), 11% to 33%, 34% to 66% (mid), 67% to 90%, and 91% to 100% (posterior). In the pre- and post-PRK cornea, the boundaries of the stromal layers were determined relative to the most anterior keratocyte layer. The post-PRK stromal thickness was compared with two pre-PRK stromal thicknesses: the *pre-PRK future unablated stroma* and the *pre-PRK full stroma* (Figure 5). In the *pre-PRK future unablated stroma*, Bowman's layer and the anterior stromal layer equal to the actual photoablation depth (as measured at 1 month post-PRK) were omitted from the analysis. In this case, the boundaries of the
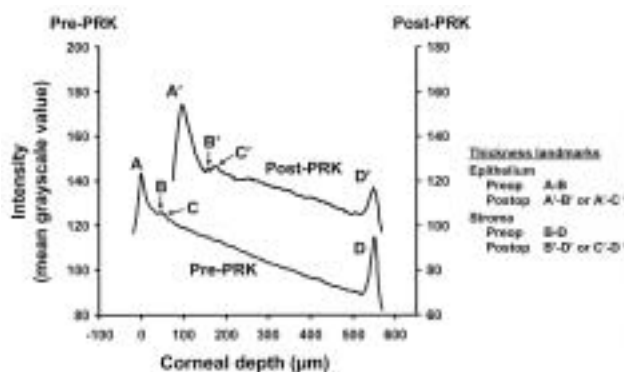

FIGURE 4

Reflected light-intensity profiles derived from confocal microscopy images of the same cornea before and after PRK. Four peaks corresponding to (A) the superficial epithelium, (B) the subbasal nerve plexus, (C) the anterior layer of keratocytes, and (D) the endothelium typically are present before PRK. Four peaks corresponding to (A') the superficial epithelium, (B') the subbasal nerve plexus, (C') the anterior layer of keratocytes (often corresponding to anterior stromal haze when present), and (D') the endothelium typically are present after PRK.
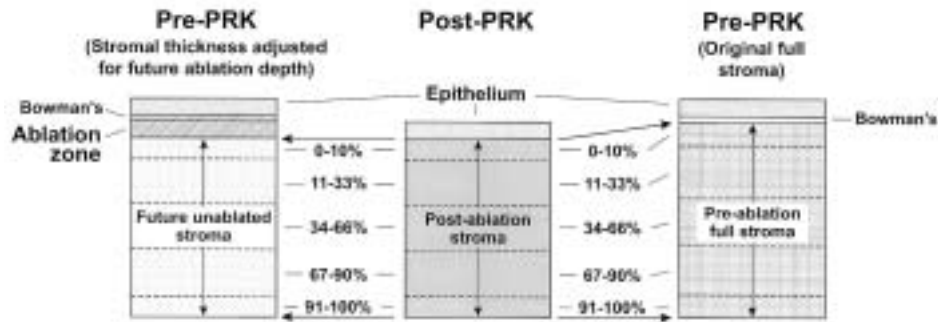
FIGURE 5

The 5 layers of the post-PRK stroma (center) and the same 5 layers of the pre-PRK future unablated stroma (left). Direct comparison of the same pre- and post-PRK tissue layers was possible by omitting the thickness of the anterior stroma equivalent to the future depth of ablation (as measured at 1 month after PRK) from the pre-PRK full stroma.

The 5 layers of the post-PRK stroma (center) and the corresponding 5 layers of the pre-PRK full stroma (right). Boundaries of the stromal layers in the pre-PRK cornea were determined relative to the most anterior keratocyte layer of the preablation full stroma.

pre-PRK stromal layers were determined relative to the most anterior keratocytes that would remain after the future PRK ablation (Figure 5, left). This allowed direct comparison of the same tissue layers in the pre- and post-PRK stroma. The *pre-PRK full stroma* included the anterior stromal layer that would later be photoablated (Figure 5, right). In this case, the boundaries of the pre-PRK stromal layers were determined relative to the most anterior keratocytes immediately posterior to Bowman's layer. The pre-PRK full stroma, the pre-PRK future unablated stroma, and the post-PRK stroma were subdivided for analysis, as described above.

We preferentially analyzed fixed-gain scans for thickness measurements, but we occasionally made thickness measurements from automatic-gain scans if they provided complete data instead. Previously, agreement was demonstrated between thickness measurements made from analysis of scans acquired by both camera modes.[44,58]

The position of the focal plane of our confocal microscope is determined by the position of the internal lens. When this lens scans linearly, the focal plane advances as a cubic polynomial from the surface of the objective, according to the specifications given by the manufacturer. We corrected depth measurements for the nonlinear separation of video images by counting the number of video frames between the frame that contained the image of the objective surface and the frame that contained the image of the epithelial surface.[44,74]

KERATOCYTE DENSITY MEASUREMENT

In each subject and at each examination, the keratocyte density was measured from images of one confocal scan of the central cornea with the camera in its automatic-gain mode. All scans were reviewed, and the single scan with the least lateral ocular movement (motion blur) and with no anterior-posterior movement of the cornea relative to the lens objective was selected for analysis.
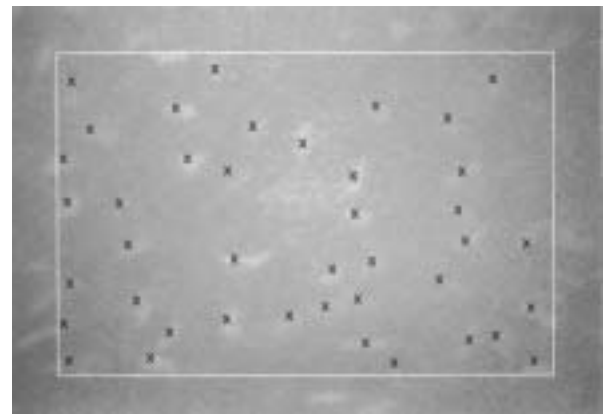

FIGURE 6

Keratocyte number and density were determined by manually counting keratocyte nuclei in selected confocal images, by using an interactive computer program. By convention, objects overlapping the edges of the bounding box were counted on only two sides of the box (left and lower sides). Bar, 100 µm.

An observer selected 2 images with well-defined bright objects (no motion blur) from each layer for analysis. In the anterior 10% of the stroma, 1 of the 2 selected images was the most anterior countable image (the first image without motion blur that contained bright keratocyte nuclei). The images were presented in random order to an observer who was masked to the subject and the examination visit. The observer manually counted bright objects (keratocyte nuclei) in the 10 selected images in 1 scan from each examination by using an interactive computer program (Figure 6).[58,73,82] The number of cells in a predetermined area was used to determine keratocyte density (cells/mm^3). The mean cell density in each layer post-PRK was compared with the mean cell density in (1) the corresponding layer of *the pre-PRK full stroma* and in (2) the same tissue layer of the *pre-PRK future unablated stroma* (stromal thickness adjusted by omitting the future ablation depth).

CORNEAL REINNERVATION

All confocal scans of sufficient quality for nerve visualization were evaluated. The scans were viewed in a randomized and masked fashion by using a personal computer with the same lighting conditions to avoid variations in contrast of the image observed on the monitor. Adequate scans were available (3 to 6 scans per eye per visit) for all eyes for all preoperative and postoperative examinations. Data obtained from these scans were averaged and used for subsequent calculations. The following variables were evaluated.

Location
Subbasal and stromal nerve fiber bundles were evaluated according to their location within the corneal thickness. Subbasal nerve fiber bundles are in close relation to the basal aspect of the basal epithelial cell layer.[50] They are anterior to Bowman's layer in the pre-PRK cornea and anterior to or within the most anterior keratocyte layer in the post-PRK cornea.[95,97] Stromal nerves included all nerves posterior to Bowman's layer in the pre-PRK cornea and all nerves posterior to the subbasal nerve fiber bundles in the post-PRK cornea. The scan position (% stromal depth) was recorded for each stromal nerve fiber bundle relative to the most anterior keratocyte layer.

Number of nerves
Nerves appeared as bright, well-defined linear structures that were sometimes branched and usually appeared in consecutive frames (Figures 3B and 3F). If the length of the visible portion of a nerve fiber bundle, including its appearance in adjacent scans, was longer than 50 µm, the nerve fiber bundle was counted. Nerve branches longer than 50 µm were also counted as separate nerves. In the subbasal region only, nerve fiber bundles were grouped into three different categories by their length: 50 to 100 µm, 100 to 200 µm, and >200 µm. The number of nerve fiber bundles located in the subbasal region and in the full-thickness stroma was recorded as the mean number per scan for each cornea for each examination.

Nerve density
A custom computer program was developed to measure the total nerve length of the subbasal nerve fiber bundles within a frame, given as micrometers of nerve fiber within an area of 0.166 mm² (ie, frame size, 0.475 × 0.350 mm) (Figure 7). All visible subbasal nerves and their branches, including their appearance in adjacent frames, were measured. The mean subbasal nerve density, expressed as µm/mm², was recorded in 3 to 6 scans per eye for each examination.

Orientation
Subbasal nerve orientation was recorded using custom software according to standard notation for specifying the axis direction of toric ophthalmic lenses (ie, the mean value of the angle formed by the nerves with respect to horizontal).[59] Usually all the nerves within the frame were found approximately in a parallel distribution. In some subbasal and stroma nerves with several short branches, the criterion had to be modified, and the main branch was given priority in defining nerve orientation of the whole frame.

Cochet-Bonnet esthesiometry was performed on each central cornea preoperatively and at 1, 2, and 3 years post-PRK. The diameter of the filament was 0.12 mm, and its length could be varied from 0 to 60 mm. The pressure applied to the cornea thus ranged from 11 to 200 mg/0.0113 mm². Each cornea was tested three times with each filament length, which was sequentially reduced in 5-mm steps starting at 60 mm. Two positive responses in three attempts at each filament length were regarded as a positive result. Corneal sensitivity threshold was the longest filament length that resulted in a positive response.[95]
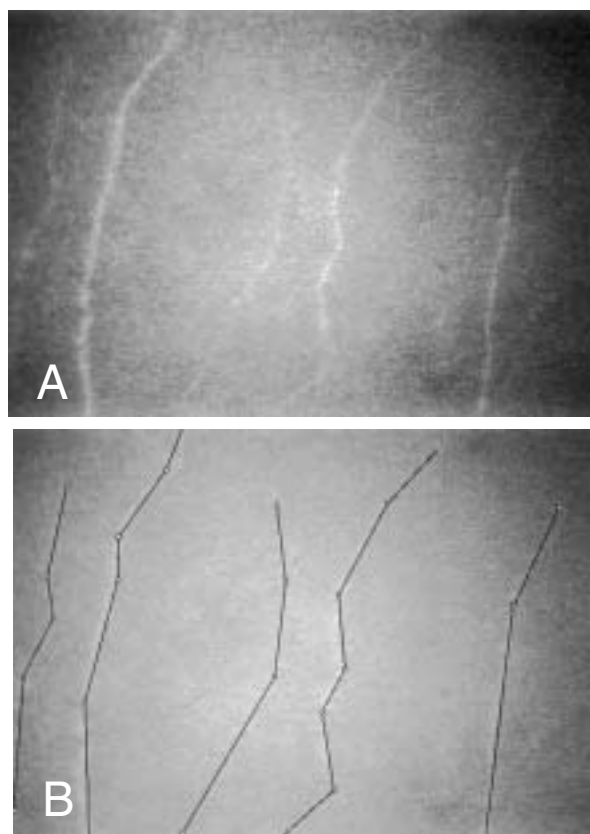

FIGURE 7
A, Confocal microscopy image shows central subbasal nerve fiber bundles as roughly parallel, bright, linear structures against the dark background of Bowman's layer. B, Tracing of subbasal nerve fiber bundles by using a custom automatic caliper tool to measure the total length (µm) and orientation (degrees) of the nerve fiber bundles within a confocal image frame (ie, 0.475 × 0.350 mm). Subbasal nerve fiber bundle density, expressed as µm/mm2, was recorded per scan per cornea at each examination.

CORNEAL HAZE

A depth-intensity profile of backscattered light from each scan was obtained by continuous through-focusing with the camera operating in its fixed-gain mode. The post-PRK intensity peak generated by the increased subepithelial light reflectivity and corresponding to anterior stromal haze was identified (Figure 4).[47,88] A quantitative measure of corneal backscattered light (corneal haze) was determined in all video images within the profile peak of anterior stromal haze by calculating the average pixel intensity in the central 160×160-µm region of each frame.[82]

Variations in sensitivity of the confocal microscope and video system were compensated for by using luminescence from a fluorescent glass standard with the camera in its fixed-gain mode before scanning each subject. The average intensity of five frames was determined at 120-frame intervals. A factor that corrected for variations in the instrument sensitivity was calculated as the ratio of the average intensity of the glass standard at an earlier time (reference day) divided by the average intensity at the time of the study. The average intensity of each image within the anterior stromal haze was multiplied by this correction factor. The average corrected intensity was accepted as a measure of anterior stromal haze in the post-PRK cornea and was compared with the average corrected intensity from the same anterior-posterior region of the pre-PRK cornea after adjusting depth of the frame for the measured photoablation depth (the anterior stroma equal to the photoablation depth, as measured 1 month after PRK, was omitted from the analysis). The pixel intensity was expressed in arbitrary units (U).

DATA ANALYSIS

Normally distributed data are given as mean ± standard deviation (SD). Groups were compared by using the paired t test if data were distributed normally or the Wilcoxon signed-rank test if they were not. Associations between continuous factors were investigated by using the Pearson product moment correlation (r_p) if data were distributed normally or the Spearman rank order correlation (r_s) if they were not. The "general estimating equation" model was investigated to account for the potential correlation between two eyes of the same individual.[190] In all cases, the conclusions were the same as the standard statistical tests, so only the standard results are provided in the paper.

P values were Bonferroni-adjusted for multiple comparisons. A P value less than 0.05 was considered statistically significant. In eyes requiring a reoperation, all data after the reoperation was excluded from analysis.

RESULTS

One thousand thirty-six confocal scans with no motion blur were identified and analyzed. No complications were encountered during the PRK procedure or in the postoperative period. Five (21%) of the 24 eyes underwent a reoperation. One eye required a reoperation at 7 months post-PRK to treat an initial undercorrection, and 4 eyes required a reoperation at 13 months post-PRK to treat myopic regression.

THICKNESS MEASUREMENTS

Epithelial Thickness

Central epithelial thickness measurements before and after PRK are shown in Tables I and II and in Figure 8. Central epithelial thickness before PRK was 44 ± 2 µm (mean ± SD). Epithelial thickness returned to preoperative levels by 1 month post-PRK (42 ± 7 µm, $P = .54$). Epithelial thickness increased 7 µm (14%) between preoperative and 3 months post-PRK ($P<.0001$) and continued to increase another 5 µm (9%) between 3 and 12 months post-PRK ($P = .02$). Epithelial thickness was unchanged between 12 and 36 months post-PRK ($P = 1.0$).

Epithelial thickening between 1 and 12 months after PRK was statistically correlated with the measured ablation depth ($r_s = 0.46$, $P = .03$), but it did not correlate with post-PRK subbasal nerve density ($r_s = 0.13$, $P = .56$) or stromal haze ($r_s = 0.20$, $P = .42$). Epithelial thickening did not correlate with the presence of activated keratocytes at 1, 3, or 6 months post-PRK ($P = .41$, .57, .61, respectively, rank sum test).

Stromal Thickness

Central stromal thickness measurements before and after PRK are shown in Tables II and III and Figure 9. The central corneal stroma was swollen 22% and 7% at 1 and 5 days post-PRK when compared to stromal thickness at 1 month after PRK. Stromal swelling was not observed by slit-lamp biomicroscopy or confocal microscopy at all examinations thereafter.

Central stromal thickness before PRK (including Bowman's layer) was 474 ± 33 µm ($n = 24$) and was significantly thinner 1 month post-PRK (429 ± 40 µm, $P<.0001$, $n = 24$). Although stromal thickness increased 8 µm between 1 month (429 ± 40 µm, $n = 24$) and 36 months post-PRK (437 ± 54 µm, $n = 19$), the difference was not significant ($P = .35$); the minimum detectable difference (MDD) was 13 µm (paired analysis, Bonferroni-adjusted for 6 comparisons, $\alpha = .05/6 = .008$, $\beta = .20$).

The intended stromal ablation depth by PRK was 46 ± 16 µm. The measured surgically induced stromal thinning between pre-PRK and 1 month post-PRK was 45 ± 16 µm. A close correlation was found between the intended and measured stromal ablation depth ($r_p = 0.91$,

TABLE I: CENTRAL EPITHELIAL THICKNESS MEASUREMENTS (µm) BEFORE AND AFTER PHOTOREFRACTIVE KERATECTOMY

SUBJECT	PREOPERATIVE (n = 24)	1 MO (n = 24)	3 MO (n = 24)	6 MO (n = 24)	12 MO (n = 23)°	24 MO (n = 19)°	36 MO (n = 19)°
1	45.2	41.8	50.2	70.0	70.2	69.6	72.2
2	43.0	40.3	53.7	68.5	63.3	66.3	70.2
3	42.3	39.4	46.8	50.0	61.1	61.1	55.9
4	42.6	47.5	46.0	44.2	55.9	50.7	53.3
5	46.8	40.3	53.7	53.3	54.0	55.4	55.9
6	42.0	38.0	48.1	46.8	53.8	°	°
7	44.9	41.6	52.0	54.0	49.4	52.0	47.6
8	40.0	38.0	55.9	52.0	52.0	53.3	52.0
9	44.2	37.2	55.5	54.1	54.6	58.1	53.3
10	45.5	36.5	41.6	45.5	49.4	47.6	54.6
11	44.2	34.0	44.8	50.7	53.3	48.1	55.9
12	40.3	35.2	52.7	50.7	49.4	51.0	52.8
13	40.8	34.0	47.6	45.8	53.8	°	°
14	44.9	52.1	58.9	50.5	58.9	58.0	52.2
15	44.3	47.8	44.2	45.0	57.2	53.3	59.8
16	45.2	44.1	44.2	54.6	58.1	56.4	61.1
17	43.6	42.0	45.8	51.4	°	°	°
18	41.6	36.4	58.5	59.8	59.0	61.5	53.9
19	39.0	35.0	59.8	57.2	54.6	°	°
20	46.8	46.7	47.7	54.6	53.3	55.1	57.9
21	47.8	51.9	52.1	50.0	49.4	61.1	68.9
22	43.6	47.0	64.9	62.4	64.2	57.2	55.5
23	44.9	52.0	59.4	57.9	62.4	°	°
24	41.6	36.4	49.4	47.5	52.8	52.0	57.9
Mean	43.6	41.5	51.4	53.2	56.1	56.2	57.4
SD	± 2.3	± 6.9	± 6.1	± 6.8	± 5.4	± 5.9	± 6.6

°Data from eyes requiring a reoperation were excluded from the analysis.

TABLE II: CENTRAL THICKNESS MEASUREMENTS (µm, MEAN ± SD) BEFORE AND AFTER PHOTOREFRACTIVE KERATECTOMY

REGION	PREOPERATIVE (n = 24)	1 MO (n = 24)	3 MO (n = 24)	6 MO (n = 24)	12 MO (n = 23)°	24 MO (n = 19)°	36 MO (n = 19)°
Epithelium	44 ± 2	42 ± 7	51 ± 6†	53 ± 7†	56 ± 5†‡	56 ± 6†	57 ± 7†
Bowman layer	14 ± 4	-	-	-	-	-	-
Stroma	460 ± 33	429 ± 44§	430 ± 43	430 ± 49	432 ± 46	434 ± 45	437 ± 54
Total cornea	517 ± 37	471 ± 45	482 ± 44	485 ± 43	490 ± 47	489 ± 45	495 ± 54

Epithelial thickness preoperatively was compared with thickness at 1, 3, 6, 12, 24, and 36 months post-PRK. Epithelial thickness at 12 months post-PRK was compared with thickness at 3 and 36 months post-PRK. Paired comparisons were completed by using the Student t test. P values were Bonferroni-adjusted for 8 comparisons (adjusted P = unadjusted P × 8). Stromal thickness at 1 month post-PRK was compared with thickness preoperatively, 3, 6, 12, 24, and 36 months post-PRK.

P values were Bonferroni-adjusted for 6 comparisons (depending on the variable). Only P values for significant differences are reported.

°Data from eyes requiring a reoperation were excluded.

†Preoperative vs 3, 6, 12, 24, and 36 months post-PRK, $P<.0001$ (Bonferroni-adjusted for 8 comparisons).

‡12 months post-PRK vs 3 months post-PRK, $P = .03$ (Bonferroni-adjusted for 8 comparisons).

§1 month post-PRK vs preoperative, $P<.0001$ (Bonferroni-adjusted for 6 comparisons).

$P<.001$, Figure 10).

Stromal thickening between 1 and 12 months after PRK did not correlate with the measured ablation depth (r_s = -0.04, P = 1.0), the post-PRK subbasal nerve density (r_s = 0.10, P = .69), or stromal haze (r_s = 0.06, P = .80). Stromal thickening did not correlate with the presence of activated keratocytes at 1, 3, or 6 months post-PRK

(P = .34, .41, and .85, respectively).

KERATOCYTE DENSITY MEASUREMENT
Central keratocyte density in the pre-PRK full stroma, the pre-PRK future unablated stroma, and the post-PRK stroma is shown in Table IV.
Post-PRK Stroma Versus Pre-PRK Full Stroma
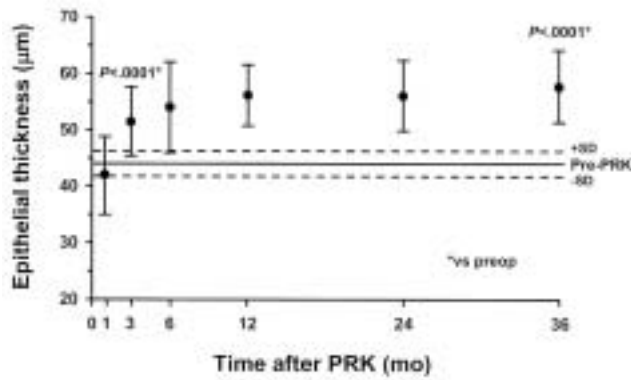
FIGURE 8

Central epithelial thickness (mean ± SD, µm) before and after photorefractive keratectomy (see Tables I and II).

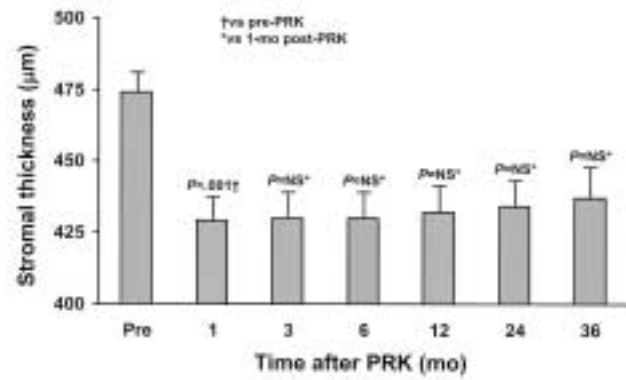**FIGURE 9**

Central stromal thickness (mean ± SD, µm) before and after photorefractive keratectomy (see Tables II and III).

TABLE III: CENTRAL STROMAL THICKNESS MEASUREMENTS (mm) BEFORE AND AFTER PHOTOREFRACTIVE KERATECTOMY							
SUBJECT	PREOPERATIVE (n = 24)	1 MO (n = 24)	3 MO (n = 24)	6 MO (n = 24)	12 MO (n = 23)†	24 MO (n = 19)†	36 MO (n = 19)†
1	420	374	376	375	375	387	363
2	416	379	382	373	371	385	367
3	457	400	387	403	394	404	409
4	458	400	388	382	382	379	393
5	529	497	500	497	491	498	519
6	516	439	447	465	462	†	†
7	484	442	434	436	437	441	445
8	445	374	384	373	372	391	380
9	460	385	386	388	389	380	373
10	504	467	469	475	478	476	486
11	522	478	503	484	494	479	503
12	486	447	455	468	460	460	461
13	489	439	437	436	432	†	†
14	452	421	424	408	417	425	417
15	438	406	410	406	400	408	416
16	486	437	437	436	439	446	469
17	461	429	429	439	†	†	†
18	450	382	371	365	364	378	368
19	450	372	371	374	394	†	†
20	540	510	508	495	500	486	499
21	506	482	489	491	497	510	520
22	481	437	443	450	467	460	454
23	471	452	444	449	471	†	†
24	465	445	450	447	459	560	464
Mean	474	429	430	430	432	434	437
SD	± 33	± 40	± 43	± 44	± 46	± 45	± 54

*Thickness includes total stroma and Bowman layer.
†Data from eyes requiring a reoperation were excluded.

In the pre-PRK full stroma, the entire full-thickness stroma was included in the analysis (Figure 5). The pre-PRK full stroma did not include Bowman's layer but did include the anterior stroma, which contains the highest population density of keratocytes in the stroma. The high-keratocyte-density anterior stroma was partially or completely removed by the excimer laser during PRK (Figure 11).

At 1 month post-PRK, keratocyte density in the anterior 0% to 10% layer was decreased 30% ($P<.0001$) compared with the anterior 0% to 10% of the pre-PRK full stroma. Keratocyte density in the anterior 0% to 10% post-PRK stromal layer never returned to preoperative levels and remained decreased 25% ($P = .002$), 41% ($P<.0001$), 40% ($P<.0001$), 43% ($P<.0001$), and 45% ($P<.0001$) at 3, 6, 12, 24, and 36 months post-PRK,
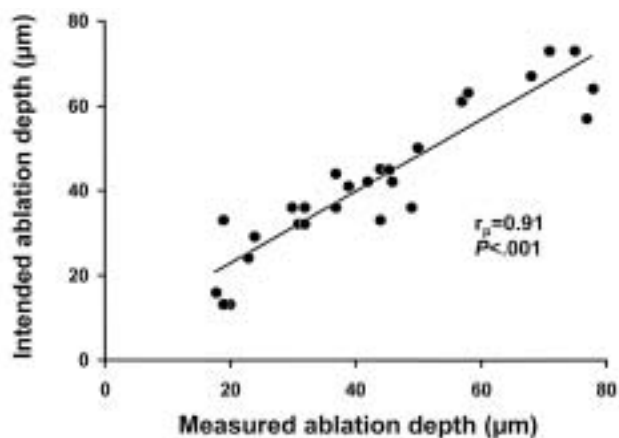
FIGURE 10

Correlation between the intended stromal ablation depth and the measured stromal ablation depth at 1 month after PRK.

respectively, compared with the anterior 0% to 10% layer of the pre-PRK full stroma (Figure 12, Table IV).

In contrast, keratocyte density in the 11% to 33%, 34% to 66%, 67% to 90%, and 91% to 100% stromal layers was increased 22% ($P<.0001$), 17% ($P = .003$), 17% ($P = .008$), and 22% ($P<.0001$), respectively, at 3 months post-PRK compared with preoperative values (Table IV). Keratocyte density in these same layers returned to preoperative levels at 6 months post-PRK and remained unchanged through 36 months post-PRK compared with the corresponding layers of the pre-PRK full stroma (Figure12, Table IV).

Post-PRK Stroma Versus Pre-PRK Future Unablated Stroma

In the pre-PRK future unablated stroma, the anterior stroma equal to the depth of ablation, as measured at 1 month post-PRK, was omitted from the analysis. This allowed direct comparison of the same tissue layers of the pre- and post-PRK stroma (Figure 5).

At 1 and 5 days post-PRK, the tandem scanning confocal microscope could not detect an anterior acellular stromal layer, if present, because of the absence of visible anterior landmarks such as the subbasal nerve plexus and the basal epithelial cells. However, at 5 days post-PRK, keratocyte density in the most anterior keratocyte layer ($17,462 \pm 3,710$ cells/mm^3, $n = 24$) was significantly less than the cell density in the next deeper analyzed image at 5% to 10% stromal depth ($23,299 \pm 3,352$ cells/mm^3, $n = 24$, $P<.01$) (Figure 13). No difference in cell density between the most anterior keratocyte layer and the next-deeper analyzed image (5% to 10% stromal depth) was observed at 1 day post-PRK ($P = .64$) or any time thereafter.

At 1 month post-PRK, the full-thickness keratocyte density ($19,861 \pm 2,447$ cell/mm^3) was 9% higher than the pre-PRK future unablated stroma ($18,110 \pm 1,947$ cells/mm^3; $P<.0001$), the result of keratocyte density in the

34% to 66% and 91% to 100% stromal layers being increased 11% ($P = .001$) and 14% ($P = .04$), respectively (Figure 11, Table IV).

At 3 months post-PRK, the full-thickness keratocyte density ($22,758 \pm 3,275$ cells/mm^3) had maximally increased 20% compared with preoperative density ($P<.0001$), the result of keratocyte density being 14% to 23% higher in all of the post-PRK stromal layers ($P<.0001$, Figure 11, Table IV).

By 6 months post-PRK, the full thickness keratocyte density ($18,612 \pm 2,406$ cells/mm^3) had returned to preoperative levels ($P = 1.0$); the MDD ($\alpha = .05$, $\beta = .20$) was 1,023 cells/mm^3. Thereafter, keratocyte density remained unchanged to 36-months post-PRK. Keratocyte density in the 11% to 33%, 34% to 66%, 67% to 90%, and 91% to 100% post-PRK stromal layers was also unchanged at 6 months post-PRK and remained unchanged to 36 months post-PRK compared with the pre-PRK future unablated stroma ($P = 1.0$, Figure 11, Figure 14).

In contrast, keratocyte density in the anterior 0% to 10% stromal layer continued to decrease 5% per year between 12 and 36 months post-PRK (Table IV). At 36 months post-PRK, keratocyte density in the anterior 0% to 10% stromal layer was reduced 15% ($17,720 \pm 4,308$ cells/mm^3) compared with the same tissue layer of the pre-PRK future unablated stroma ($20,930 \pm 2,819$ cells/mm^3; $P = .02$; Figure 11, Figure 14).

KERATOCYTE MORPHOLOGY

Keratocyte nuclei appeared as bright oval or bean-shaped objects against a dark background in preoperative confocal images (Figures 3 and 6). Cellular processes were not evident. Consistent with previous studies of normal corneas, the preoperative anterior keratocytes were smaller, more numerous, and more tightly packed than the posterior keratocytes.[44,59,60]

At 1 day post-PRK, keratocyte nuclei were the same size, shape, and reflectivity as quiescent keratocytes in the corresponding layer of the preoperative cornea. Large, highly reflective cells, thought to represent activated keratocytes, were not seen at this time. Keratocyte nuclei in the most anterior keratocyte layer were more numerous in corneas with shallow ablations and less numerous in corneas with deep ablations, consistent with the expected density at the same adjusted stromal depth in the preoperative cornea (Figure 15).

At 5 days post-PRK, 4 (17%) of 24 eyes had large, brightly reflective keratocyte nuclei in the anterior stroma that were associated with prominent interconnecting cell processes. These large, highly reflective cells have been interpreted to represent activated keratocytes.[47,88,89,157] Some of the highly reflective keratocytes appeared considerably larger than others, but all seemed to be

TABLE IV: CENTRAL KERATOCYTE DENSITY (MEAN ± SD, CELLS/mm³) BEFORE AND AFTER PHOTOREFRACTIVE KERATECTOMY

STROMAL LAYER (% STROMAL THICKNESS)	PRE-PRK FULL STROMA (n = 24)	PRE-PRK FUTURE UNABLATED STROMA (n = 24)	1 DAY (n = 24)	5 DAYS (n = 24)	1 MO (n = 24)	3 MO (n = 24)	6 MO (n = 24)	12 MO (n = 23)°	24 MO (n = 19)°	36 MO (n = 19)°
Full-thickness	19,608 ± 2,236	18,110 ± 1,947	18,835 ± 3,207	18,718 ± 2,653	19,861 ± 2,447§	22,758 ± 3,275†§	18,612 ± 2,406†	17,304 ± 2,572†	17,686 ± 2,609†	17,372 ± 2,443†
Regional densities:										
0-10% (anterior)	32,380 ± 5,848	20,930 ± 2,819	22,589 ± 4,908†	22,456 ± 3,467†	22,813 ± 4,001†	24,434 ± 3,636‡§	19,100 ± 2,569†	19,560 ± 3,795†	18,613 ± 4,112†	17,720 ± 4,308§¶
11%-33%	18,840 ± 2,265	18,492 ± 2,534	20,838 ± 3,685	19,049 ± 2,898	20,598 ± 3,242	24,046 ± 3,411†§	20,107 ± 3,445	18,228 ± 2,547	17,786 ± 4,811	18,757 ± 3,164
34%-66% (mid)	18,235 ± 3,579	17,038 ± 2,623	18,272 ± 3,375	17,185 ± 3,487	19,136 ± 2,385¶	22,007 ± 3,792†§	18,128 ± 3,489	16,531 ± 3,938	17,462 ± 3,580	17,235 ± 2,752
67%-90%	18,368 ± 2,625	17,592 ± 4,123	17,003 ± 2,989	17,937 ± 3,411	18,968 ± 2,313	22,000 ± 3,975†§	17,757 ± 2,781	16,352 ± 3,458	16,705 ± 3,983	16,917 ± 2,593
91%-100% (posterior)	17,402 ± 3,603	17,204 ± 3,590	16,666 ± 3,670	18,163 ± 3,081	20,035 ± 2,858†¶	22,407 ± 3,352†§	18,380 ± 3,227	16,849 ± 2,985	17,084 ± 3,141	16,417 ± 2,859

Keratocyte density at 1 day, 5 days, and 1, 3, 6, 12, 24, and 36 months post-PRK was compared to cell density of the pre-PRK full stroma and the pre-PRK future unablated stroma. Paired comparisons were completed by using the Student t test. *P* values were Bonferroni-adjusted for 8 comparisons (adjusted *P* = unadjusted *P* × 8). Only *P* values for significant differences are reported.

°Data from eyes requiring a reoperation were excluded.

†*P*<.0001, post-PRK keratocyte density compared to pre-PRK full stroma keratocyte density (Bonferroni-adjusted for 8 comparisons).

‡*P*<.01, post-PRK keratocyte density compared to pre-PRK full stroma keratocyte density (Bonferroni-adjusted for 8 comparisons).

§*P*<.0001, post-PRK keratocyte density compared to pre-PRK future unablated stroma keratocyte density (Bonferroni-adjusted for 8 comparisons).

¶*P*<.05, post-PRK keratocyte density compared to pre-PRK future unablated stroma keratocyte density (Bonferroni-adjusted for 8 comparisons).
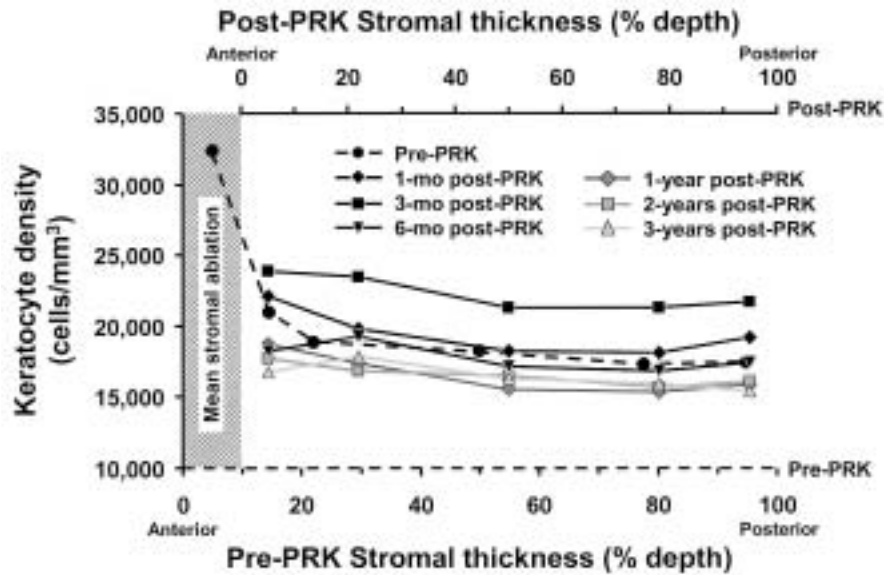
FIGURE 11

Comparison of pre- and post-PRK keratocyte density. PRK photoablation removes anterior stroma (hatched lines) containing a high keratocyte population, and this high keratocyte density is not reconstituted in the post-PRK anterior stroma.
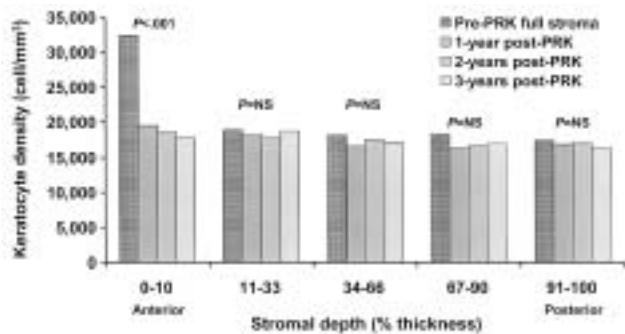

FIGURE 12

Comparison of keratocyte density in the pre-PRK full stroma to keratocyte density in the post-PRK stroma at 1, 2, and 3 years after surgery. The pre-PRK full stroma includes the entire full-thickness stroma in the analysis (Figure 5).

larger than the preoperative quiescent keratocytes. The number of eyes with large, highly reflective "activated" anterior keratocytes peaked at 3 months after PRK. By 12 months after PRK, keratocyte morphology was similar to preoperative and large, bright activated keratocyte nuclei were no longer seen (Figure 16). When large, bright activated keratocytes were identified, they were always seen in the first visualized keratocyte layer and extended posteriorly to depths ranging from 10 to 57 μm (Table V). Activated keratocytes were never seen in the middle or posterior stroma in any of the eyes.

At 5 days post-PRK, 3 (13%) of 24 eyes had occasional small, bright objects that were thought to represent inflammatory cells (Figure 16). Similar small bright objects were not seen at any other examination.
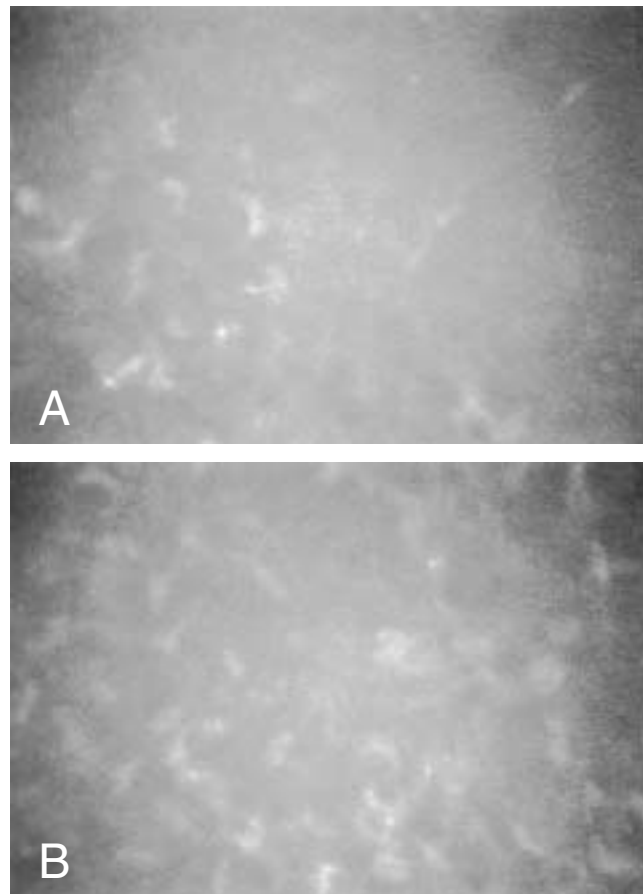

FIGURE 13

Confocal microscopy images of anterior keratocytes at 5 days post-PRK in the same patient (intended ablation depth of 43 μm). A, The most anterior keratocyte layer demonstrates decreased cell density compared with B, the keratocyte layer at 8% stromal depth..
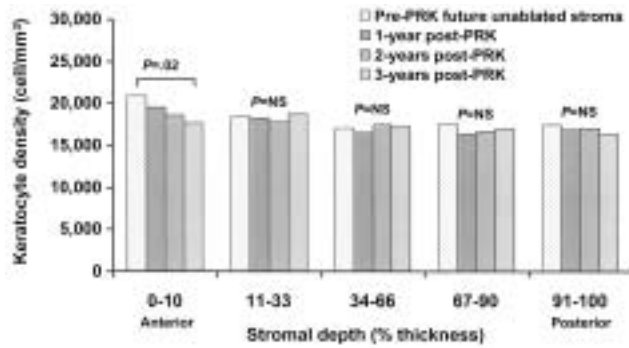
FIGURE 14
Comparison of keratocyte density in the pre-PRK future unablated stroma to keratocyte density in the post-PRK stroma at 1, 2, and 3 years post-PRK. The pre-PRK future unablated stroma adjusted thickness for the future ablation depth by subtracting stromal thickness at 1 month post-PRK from preoperative thickness (Figure 5). This allowed direct comparison of the same tissue layers in the pre- and post-PRK stroma.

CORNEAL HAZE

Clinical stromal haze at 1 month post-PRK was subjectively graded as trace (defined as haze seen only with broad-beam illumination) in 3 (13%) of 24 eyes and clear in 21 eyes (87%). At 3 and 6 months post-PRK, haze was graded as trace in 1 (4%) of the 24 eyes, grade 1 (defined as haze visible by direct slit-beam illumination) in 1 eye (4%), and clear in 22 (92%) eyes. All (100%) eyes were graded as clear at 12, 24, and 36 months post-PRK.

Objective confocal microscopy haze estimates are shown in Table VI. The confocal microscopy haze estimate did not correlate with subjective haze grading by slit-lamp biomicroscopy at 1, 3, and 6 months post-PRK ($r = 0.19$, $P = .29$, $n = 72$ postoperative visits). At 1, 3, and 6 months post-PRK, 55 (85%) of the 65 corneas that clinically appeared clear at the slit-lamp examination had increased confocal microscopy haze estimates, compared with their preoperative examination, demonstrating the ability of the confocal microscope to detect subtle alterations in post-PRK corneal light backscattering (ie, subclinical haze).

At 1 month post-PRK, 20 (83%) of the 24 corneas demonstrated an increase in corneal light backscattering. At 3 and 6 months post-PRK, 23 (96%) and 16 (67%) corneas demonstrated an increase in corneal light backscattering despite the intensity of backscattered light at 6 months not differing statistically from preoperative values.

Correlations between confocal microscopy haze estimates and myopic regression are shown in Table VII. The measure of the haze estimate at 1 and 3 months post-PRK was significantly correlated with the measured photoablation depth ($r_s = -0.48$, $P = .02$ and $r_s = -0.52$, $P = .01$, respectively) but not correlated with the presence of activated keratocytes ($P = .57$ and .25, rank sum test). The cumulative measure of the corneal haze estimate at
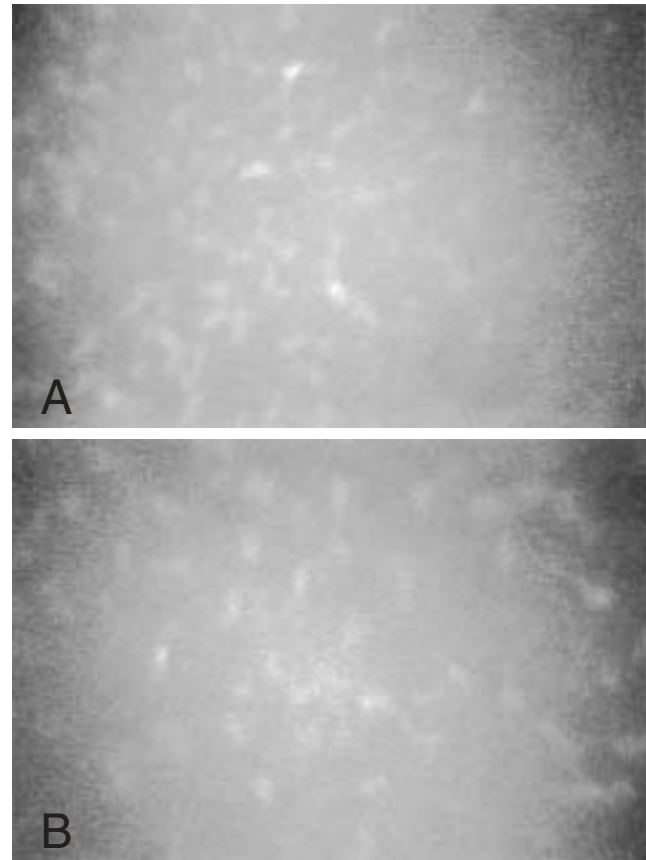

FIGURE 15
Confocal microscopy images of the (A) most anterior keratocyte layer 1 day after an intended stromal ablation depth of 15 µm and (B) after an intended stromal ablation depth of 43 µm. At 1 day post-PRK, the keratocyte morphology and density are similar to the corresponding keratocyte layer in the pre-PRK stroma.

12 months after PRK was not correlated with the subbasal nerve fiber bundle density ($r_s = 0.29$, $P = .22$).

CORNEAL REINNERVATION

Corneal Sensation

The mean central corneal sensitivity, as measured by Cochet-Bonnet esthesiometry, was 58 ± 5 mm, 57 ± 7 mm, and 58 ± 5 mm at 12, 24, and 36 months post-PRK and was unchanged compared with the mean central corneal sensitivity before PRK (60 ± 0 mm, $P = .62$).

Subbasal nerve Fiber Bundles

Location. Subbasal nerve fiber bundles were identified in 4 (17%) of 24 eyes at 1 month post-PRK, in 14 eyes (58%) at 3 months post-PRK, and in all eyes (100%) at pre-PRK and at 6, 12, 24, and 36 months post-PRK.

At 1 and 3 months post-PRK, nerve fiber bundles were perceived within the epithelial-stromal interphase in images containing both epithelial cells and keratocyte nuclei. At 6, 12, 24, and 36 months post-PRK, nerve fiber bundles were found occasionally in the epithelial-stromal
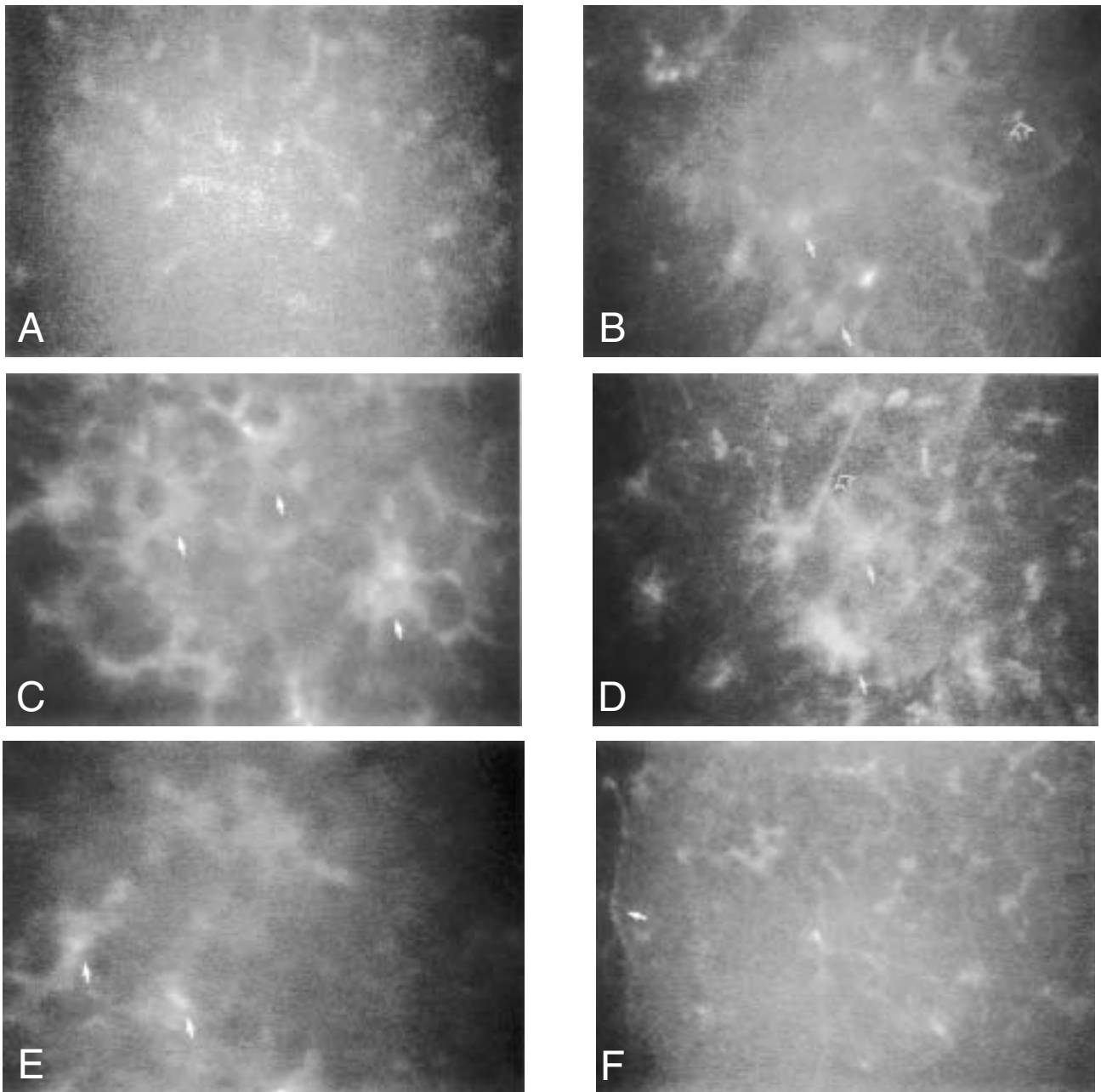
FIGURE 16

Confocal images of the first visualized keratocyte layer in the same subject after PRK (intended stromal ablation depth of 44 µm). A, One day post-PRK. The keratocyte nuclei are similar in size, shape, and reflectivity to normal quiescent keratocyte nuclei at same stromal depth preoperatively. B, Five days post-PRK. Highly reflective cells presumably representing activated keratocytes are first identified (arrows). Small, bright objects presumably representing inflammatory cells are occasionally present (open arrow). C, One month post-PRK. Large, bright, activated keratocyte nuclei with easily visible cytoplasmic process (arrows). D, Three months post-PRK. Peak prevalence of activated keratocytes (arrows). Deposition of ECM can be seen as areas of increased reflectivity beside keratocyte nuclei. A linear nerve fiber bundle is marked by an open arrow. E, Six months post-PRK. Activated keratocyte nuclei persist (arrows). F, Twelve months post-PRK. Quiescent keratocyte nuclei and regenerated slender subbasal nerve fiber bundles (arrow).

interface but were more likely to be associated with the most anterior keratocyte nuclei (Figure 17).

Density. Subbasal nerve fiber bundle density is shown in Figure 18 and Table VIII. After PRK, the subbasal nerve fiber bundle density decreased by 98% at 1 month post-PRK (148 ± 359 µm/mm²) compared with the density before PRK (6,944 ± 1,935 µm/mm²; $P<.0001$). Density remained decreased by 87% ($P<.001$), 75% ($P<.001$), and 60% ($P<.001$) at the 3, 6, and 12 months post-PRK compared with preoperative values. By 24 months after PRK, subbasal nerve fiber bundle density (6,232 ± 1,761 µm/mm²) was not significantly different

TABLE V: NUMBER OF EYES WITH ACTIVATED KERATOCYTES AND THEIR ANTERIOR STROMAL DEPTH AFTER PHOTOREFRACTIVE KERATECTOMY

MEASUREMENT	5 DAYS (n = 24)	1 MO (n = 24)	3 MO (n = 24)	6 MO (n = 24)	12 MO (n = 23)°	24 MO (n = 19)°	36 MO (n = 19)°
No.	4	13	17	7	0	0	0
(%)	(17)	(54)	(71)	(29)	(0)	(0)	(0)
Stromal depth, † µm	23.4 ± 5.7	23.7 ± 12.5	22.6 ± 9.9	18.5 ± 7.0	-	-	-

°Data from eyes requiring a reoperation were excluded from analysis.
†Posterior extension from the subbasal nerve plexus or the first anterior keratocytes.

TABLE VI: CONFOCAL MICROSCOPY HAZE ESTIMATE°

TIME (MO)	HAZE ESTIMATE	P†
Preoperative	118 ± 18	-
1	121 ± 17	<.001
3	122 ± 18	<.001
6	123 ± 26	.16
12	120 ± 13	.44
24	120 ± 14	.75
36	120 ± 16	.99

°Average pixel intensity of corneal backscattered light expressed as Mean ± SD in arbitrary units (U).
†Bonferroni-adjusted Student t test for 6 comparisons (adjusted P = unadjusted $P \times 6$) comparing the confocal microscopy haze estimate before PRK to the confocal microscopy haze estimate after PRK. All other similar comparisons were not significant.

TABLE VII: CORRELATIONS BETWEEN CONFOCAL MICROSCOPY CORNEAL HAZE ESTIMATE AND REFRACTIVE REGRESSION

TIME (MO)	r_s°	P
1	0.41	.04
3	0.48	.02
6	0.40	.07
12	0.53	.02
24	0.53	.03
36	0.08	.77

° Spearman rank order correlation.

from preoperative values (P = 1.0) and remained unchanged at 36 months after PRK (6,506 ± 2,223 µm/mm²; P = 1.0); the MDD (α= .05, β = .20) was 1,871 µm/mm² and 2,083 µm/mm²), respectively (Figure 18).

Correlation between the regenerated subbasal nerve plexus density and keratocyte density is shown in Table IX.

Number. The number of subbasal nerve fiber bundles at each observation time is given in Table X. Consistent with nerve fiber bundle density, the number of subbasal nerve fiber bundles was decreased at each postoperative examination until 24 and 36 months after PRK when the numbers were not significantly different from the numbers before PRK (3.4 and 3.5, respectively, P=1.0); the MDD (α = .05, β =.20) was 1.0 and 1.4 at 24 and 36 months, respectively.

The mean number of long nerve fiber bundles (> 200 µm) was not significantly different from preoperative values by 24 months after PRK (2.1 ± 1.3, P = .70); the MDD (α = .05, β = .20) was 1.2. The mean number of medium nerve fiber bundles (101 to 200 µm) was not significantly different from preoperative values by 6 months after PRK (P = .50), the MDD (α = .05, β = .20) was 0.5. The mean number of short nerve fiber bundles

(50 to 100 µm) was not significantly different from preoperative values at all post-PRK examinations; the MDD was 0.4 at all examinations (α = .05, β = .20).

Orientation. The orientation of the central subbasal nerve fiber bundles before and after PRK is shown in Table XI. At 3 and 6 months after PRK, the horizontal to oblique orientation of the regenerated subbasal nerve fiber bundles differed significantly from the preoperative vertical orientation (P<.001 and P<.001, respectively). At 12 months after PRK, the vertical orientation of the regenerated subbasal nerve fiber bundles was reestablished (94 ± 47°), and they remained vertically oriented at 24 and 36 months after PRK (89 ± 33° and 105 ± 41°, respectively).

Morphology. Subjectively, the subbasal nerve fiber bundles after PRK were thinner and more tortuous than before PRK (Figure 17). No quantitative measurement of nerve fiber bundle width was made.

Stromal Nerve Fiber Bundles

The mean and median number of stromal nerve fiber bundles and their percentage of stromal depth before and after PRK are given in Table XII. No stromal nerve fiber bundles were identified deeper than 60% stromal depth before or after PRK. The mean and median number of central stromal nerve fiber bundles was unchanged at all
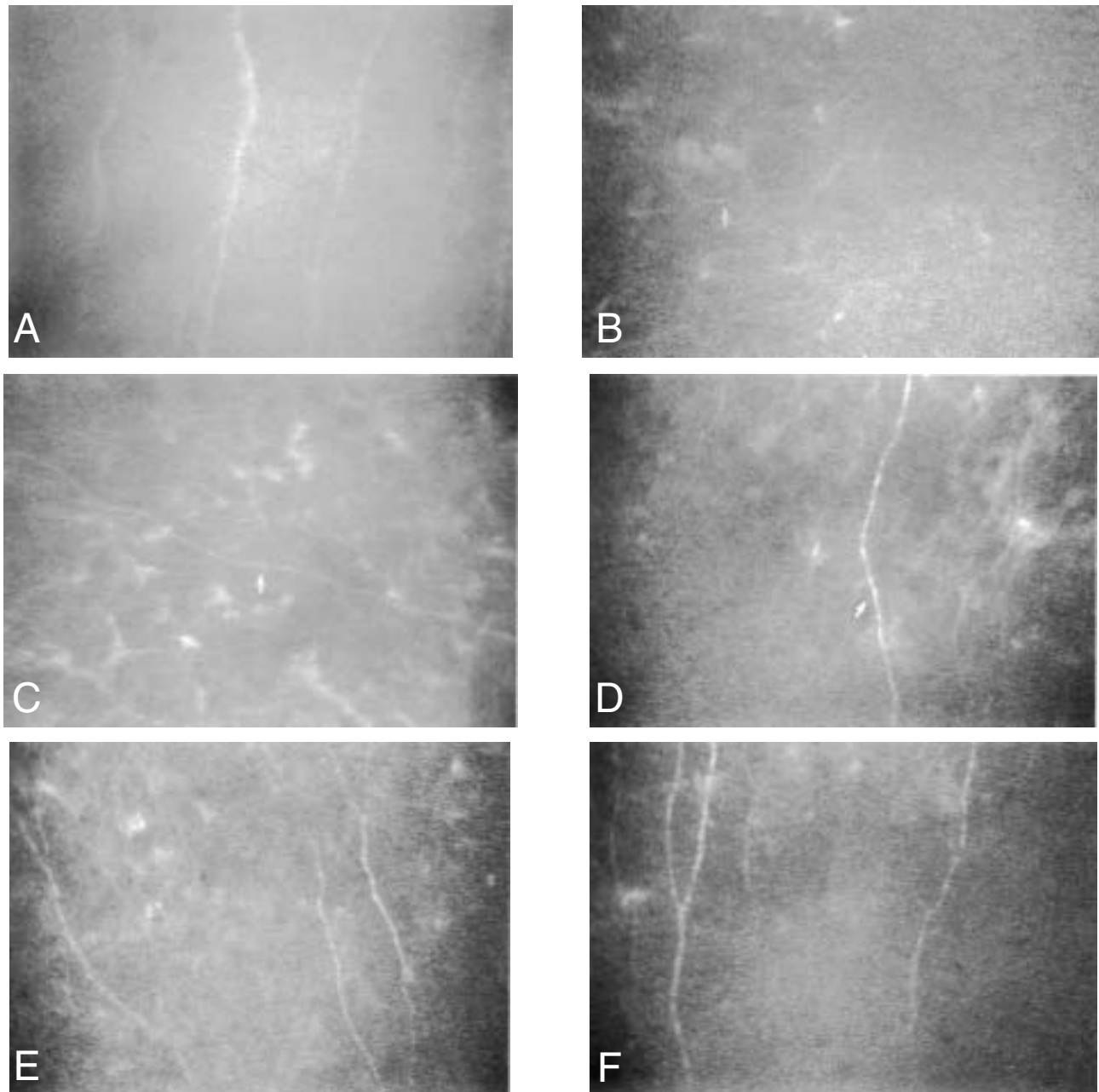
FIGURE 17

Confocal images of central subbasal nerve fiber bundles (arrows) in the same subject (A) before PRK and at 3 months(B), 6 months(C), 12 months(D), 24 months (E), and 36 months (F) post-PRK. Nerve bundles at all post-PRK examinations were subjectively thinner compared with preoperative. Nerve fiber bundles were horizontally oriented up to 6 months after PRK before returning to their preoperative vertical orientation at 12 months after PRK.

post-PRK examinations compared with preoperative values.

Beginning at 6 months after PRK, the regenerated stromal nerves rose anteriorly to the subbasal region and the stroma immediately posterior to the epithelium and directly sprouted new subbasal nerve fiber bundles (Figure 19). The number of eyes with this particular neural reorganization increased over time: 3 (13%) of 24 eyes at 6 months, 4 (17%) of 23 eyes at 12 months, 8 (42%) of 19 eyes at 24 months, and 13 (68%) of 19 eyes at

36 months after PRK. Subbasal nerve fiber bundles that directly arose from regenerated anterior stromal nerves were oriented vertically or obliquely with respect to the cornea. This pattern of neural reorganization was not associated with the presence of activated keratocytes at 6 months post-PRK (P = .53) or post-PRK subbasal nerve density at 6, 12, 24, or 36 months post-PRK (P>.57).

Aberrant regeneration of anterior stromal nerves was observed in one eye (subject 19) 1 year after a PRK reoperation to correct a regression of –1.00 D (12-µm stromal
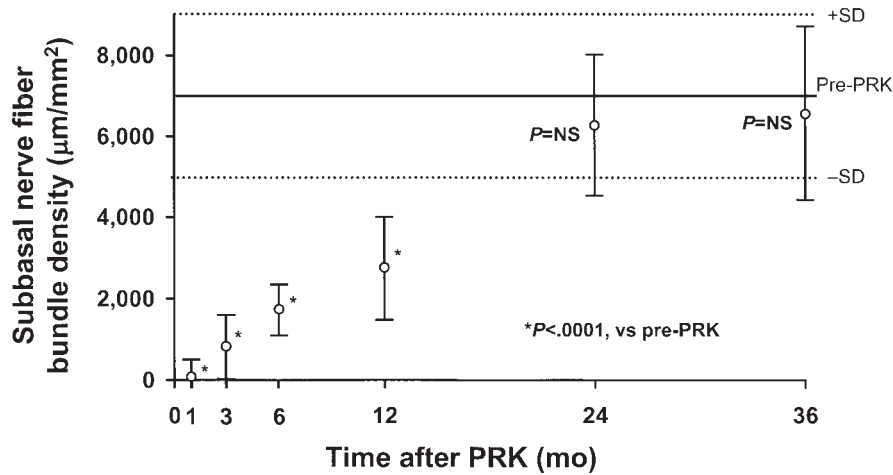
FIGURE 18

Subbasal nerve fiber bundle density (Mean ± SD, µm/mm²) in the central cornea before and after photorefractive keratectomy (see Table VIII).

TABLE VIII: CENTRAL SUBBASAL NERVE FIBER BUNDLE DENSITY (µm/mm²) BEFORE AND AFTER PHOTOREFRACTIVE KERATECTOMY

SUBJECT	PREOPERATIVE (n = 24)	1 MO (n = 24)	3 MO (n = 24)	6 MO (n = 24)	12 MO (n = 23)°	24 MO (n = 19)°	36 MO (n = 19)°
1	4421	986	1347	1588	2695	5462	6286
2	4734	0	1540	1420	2135	4595	5756
3	9113	0	1342	1516	1233	4277	5762
4	5829	0	1100	1492	1570	6995	2376
5	7392	0	0	1576	1636	4271	4854
6	6208	0	0	1997	3795	°	°
7	7429	0	1588	1119	1474	4198	4136
8	5907	0	0	1125	1859	10352	8168
9	7651	0	0	2821	1696	5792	6027
10	6009	1317	1001	1245	2039	4830	3808
11	4806	0	848	1925	1967	3567	4866
12	9654	0	1209	2406	4974	8421	10057
13	9660	686	1901	908	1660	°	°
14	11561	0	583	1689	5444	7711	6334
15	7609	553	1221	1973	2803	6358	7627
16	7802	0	1979	1083	4559	7218	10418
17	7507	0	1185	1504	°	°	°
18	7302	0	2861	1281	3020	7753	9738
19	9395	0	0	2839	4180	°	°
20	7146	0	0	2827	2803	6629	5811
21	4932	0	0	1456	5143	6623	9426
22	4734	0	716	3242	2502	5474	5642
23	5143	0	499	1600	2105	°	°
24	4704	0	0	1510	2887	7886	6532
Mean	6,944	148	872	1,756	2,790	6,232	6,506
SD	± 1,935	± 359	± 935	± 633	± 1,280	± 1,761	± 2,223
Median	7,224	0	782	1,546	2,502	6,358	6,027

°Data from eyes requiring a reoperation were excluded.

ablation). The PRK reoperation was performed 13 months after the original PRK. The aberrant anterior stromal nerves demonstrated a coiled course and irregular branching pattern, were identified 22 µm deep to the most anterior keratocyte layer, and remained unchanged to 2 years after PRK reoperation (Figure 20). No nerves in the stroma anterior to the aberrant nerves and no subbasal nerve fiber bundles were identified 1 year after PRK reoperation. By 2 years after PRK reoperation, stromal nerves that supplied a now visible subbasal plexus were identified. Corneal sensation measured by Cochet-Bonnet esthesiometry, was 60 mm and 60 mm at 12 and

eyes demonstrated a myopic shift, 5 eyes (22%) demonstrated no refractive shift, and 0 eyes (0%) demonstrated a hyperopic shift. One eye underwent a reoperation for an initial undercorrection of –0.75 D at 7 months after PRK. Four eyes underwent a reoperation at 13 months after PRK because of a mean myopic regression of –0.63 D (range, –0.50 to –1.00 D).

Correlation between refractive regression at 12 months after PRK and changes in thickness between 1 and 12 months is shown in Table XIII. Refractive regression at 12 months did not correlate with the measured ablation depth ($r_s = 0.16$, $P = .46$), the post-PRK subbasal nerve fiber bundle density ($r_s = -0.38$, $P = .08$), but did

TABLE X: NUMBER OF CENTRAL SUBBASAL NERVE FIBER BUNDLES [MEAN ± SD (MEDIAN)] BEFORE AND AFTER PHOTOREFRACTIVE KERATECTOMY

CATEGORY	PRE-PRK (n = 24)	1 MO (n = 24)	3 MO (n = 24)	6 MO (n = 24)	12 MO (n = 23)°	24 MO (n = 19)°	36 MO (n = 19)°
Total NFB 50 to > 200µm	4.0 ± 1.7 (3.8)	0.3 ± 0.8† (0.0)	0.4 ± 0.4† (0.5)	0.9 ± 0.5† (1.0)	1.9 ± 0.8† (1.5)	3.4 ± 1.2 (3.3)	3.5 ± 1.2 (3.5)
Long NFB > 200 µm	3.1 ± 1.5 (3.0)	0 ± 0.0† (0.0)	0.2 ± 0.3† (0.0)	0.2 ± 0.4† (0.0)	0.7 ± 0.9† (0.5)	2.1 ± 1.3 (1.5)	2.0 ± 1.3 (2.0)
Medium NFB 101 to 200 µm	0.8 ± 0.6 (0.5)	0.1 ± 0.4† (0.0)	0.1 ± 0.3† (0.0)	0.5 ± 0.5 (0.5)	0.8 ± 0.6 (0.5)	0.8 ± 0.4 (0.5)	0.9 ± 0.5 (1.0)
Short NFB 50 to 100 µm	0.1 ± 0.5 (0.0)	0.1 ± 0.6 (0.0)	0.2 ± 0.2 (0.0)	0.2 ± 0.3 (0.0)	0.4 ± 0.4 (0.5)	0.5 ± 0.5 (0.5)	0.6 ± 0.5 (0.5)

NFB, nerve fiber bundle.
°Data from eyes requiring a reoperation were excluded from analysis.
†$P<.0001$, Bonferroni-adjusted paired Student t test for 6 comparisons (adjusted P = unadjusted $P \times 6$) comparing the number of NFBs before PRK to the number of NFBs after PRK. All other similar comparisons were not significant.

TABLE XI: ORIENTATION OF CENTRAL SUBBASAL NERVE FIBER BUNDLES (MEAN ± SD) BEFORE AND AFTER PHOTOREFRACTIVE KERATECTOMY

MEASUREMENT	PREOPERATIVE (n = 24)	1 MO (n = 24)	3 MO (n = 24)	6 MO (n = 24)	12 MO (n = 23)°	24 MO (n = 19)°	36 MO (n = 19)°
Orientation, degrees	90 ± 31	16 ± 27	7 ± 43†	22 ± 40†	94 ± 47	89 ± 33	105 ± 41

°Data from eyes requiring a reoperation were excluded from the analysis.
†$P<.001$, Bonferroni-adjusted paired Student t test for 6 comparisons (adjusted P = unadjusted P x 6) comparing postoperative nerve fiber bundle orientation with preoperative nerve fiber bundle orientation. All other similar comparisons were not significant.

24 months after PRK reoperation, respectively.

REFRACTIVE CHANGES

The mean manifest spherical equivalent before and after PRK is shown in Figure 21. All eyes had a significant decrease in myopia in the first postoperative month ($P<.0001$). The change in refractive error between 1 and 12 months after PRK was –0.41 ± 0.30 D (range, 0 to –1.00 D). By 12 months after PRK, 18 (78%) of the 23

correlate with confocal microscopy haze estimates ($r_s = 0.53$, $P = .02$).

DISCUSSION

Surgical wounding of the cornea by excimer laser PRK alters the normal structure, cellularity, and innervation of the cornea. Biologic variability in the subsequent wound healing response is thought to be a major factor

CATEGORY	**PRE-PRK** (n = 24)	**1 MO** (n = 24)	**3 MO** (n = 24)	**6 MO** (n = 24)	**12 MO** (n = 23)†	**24 MO** (n = 19)†	**36 MO** (n = 19)†	**P‡**
Full stroma	3.0 ± 2.0 (3.0)	2.8 ± 2.1 (3.0)	2.8 ± 1.9 (2.0)	3.2 ± 1.9 (3.0)	2.7 ± 2.4 (2.0)	3.3 ± 2.5 (3.0)	3.5 ± 2.1 (3.0)	1.0§
Anterior 0-33%	2.0 ± 1.1 (2.0)	1.8 ± 1.3 (2.0)	1.9 ± 1.4 (2.0)	2.2 ± 1.5 (2.0)	1.7 ± 1.7 (1.0)	2.3 ± 1.9 (2.0)	2.3 ± 1.7 (2.0)	1.0§
Middle 11%-66%	1.0 ± 1.1 (0.5)	1.0 ± 1.0 (1.0)	0.9 ± 1.0 (0.5)	1.0 ± 1.1 (1.0)	1.0 ± 1.6 (1.0)	1.0 ± 1.2 (1.0)	1.2 ± 1.2 (1.0)	1.0§
Posterior 67%-100%	0 ± 0 (0)	0 ± 0 (0)	0 ± 0 (0)	0 ± 0 (0)	0 ± 0 (0)	0 ± 0 (0)	0 ± 0 (0)	1.0§

TABLE XII: NUMBER OF STROMAL NERVE FIBER BUNDLES [MEAN ± SD (MEDIAN)] BEFORE AND AFTER PRK

°Excludes the stromal layer subsequently ablated. If this layer is included (pre-PRK full stroma), then the values are 3.2 ± 2.2 (3.0).
†Data from eyes requiring a reoperation were excluded from analysis.
‡Bonferroni-adjusted paired t test for 6 comparisons (adjusted P = unadjusted P ¥ 6).
§ All times post-PRK were not significant from pre-PRK.

TABLE XIII: CORRELATIONS BETWEEN REFRACTIVE REGRESSION AT 12 MONTHS AND CHANGES IN THICKNESS BETWEEN 1 AND 12 MONTHS

REGION	r_s	P	n
Epithelium	0.56	.006	23
Stroma	−0.39	.08	23
Cornea	0.79	<.001	23

limiting the predictability of the outcome of refractive surgical procedures such as PRK. The corneal wound healing response is exceedingly complex, and understanding this process seems to become more difficult with increasing knowledge. Nevertheless, some of the recuperative properties that ultimately reestablish organizational coherence and function are illustrated in this prospective longitudinal confocal microscopy in vivo study.

EPITHELIAL THICKNESS

Biologic diversity in the epithelial healing response is demonstrated by the variable thickness of regenerated epithelium reported in human and animal corneas after PRK. Histologic studies on animal[123,165,167,191] and human eyes,[171-173,175,182,192] as well as in vivo studies with the confocal microscope or an optical pachometer,[95,101,193-195] have found that the healed central epithelium is thicker after PRK. Epithelial hypertrophy after PRK has been shown to be due to both vertical elongation of the basal cells and an increase in the number of superficial cell layers.[123,191,195] Similar epithelial thickening has been noted after LASIK.[42,45,196,197] In contrast, some histologic studies[87,128,169,170] and one in vivo study[110] have found the thickness of the regenerated central epithelium to be unchanged after

PRK. Interpretation of data from previous studies with respect to epithelial thickness can be problematic because of variation in physical and clinical variables or the absence of a pre-PRK examination.

In the current longitudinal in vivo study, the central epithelium was shown to return to preoperative thickness by 1 month after PRK. Consistent with most previous PRK in vivo studies,[95,101,193-195] the regenerated central epithelium continued to thicken progressively in the first year after PRK. At 12 months after PRK, the central epithelium was 21% thicker than preoperatively, presumably because of epithelial hyperplasia. New long-term data provided by this study yield statistical justification to conclude that a thicker epithelium stabilizes in thickness by 12 months after PRK and thereafter remains unchanged to at least 36 months.

Epithelial hyperplasia is noted often in corneal diseases associated with stromal loss as the regenerating epithelium attempts to fill and restore a smooth surface to the cornea.[198] Epithelial hyperplasia after PRK has been associated with deep stromal ablation depths and small ablation zones (4.5 to 5.0 mm) in which there are greater dioptric changes at the edge of the ablation zone.[110,192,195] Large ablation zones (6.0 mm), with presumably smoother edge contours, have been associated with less change in epithelial thickness.[110] The biologic advantage of epithelial thickening after PRK is unclear. Dierick and Missotten[199] suggested a tension model in which the epithelium attempts to restore the original curvature of the cornea. Reinstein and colleagues[42] demonstrated that the epithelium varied in thickness to compensate for variable underlying stromal surface abnormalities. The epithelium thinned over protuberances and thickened over defects in the stroma—an overall effect that tended
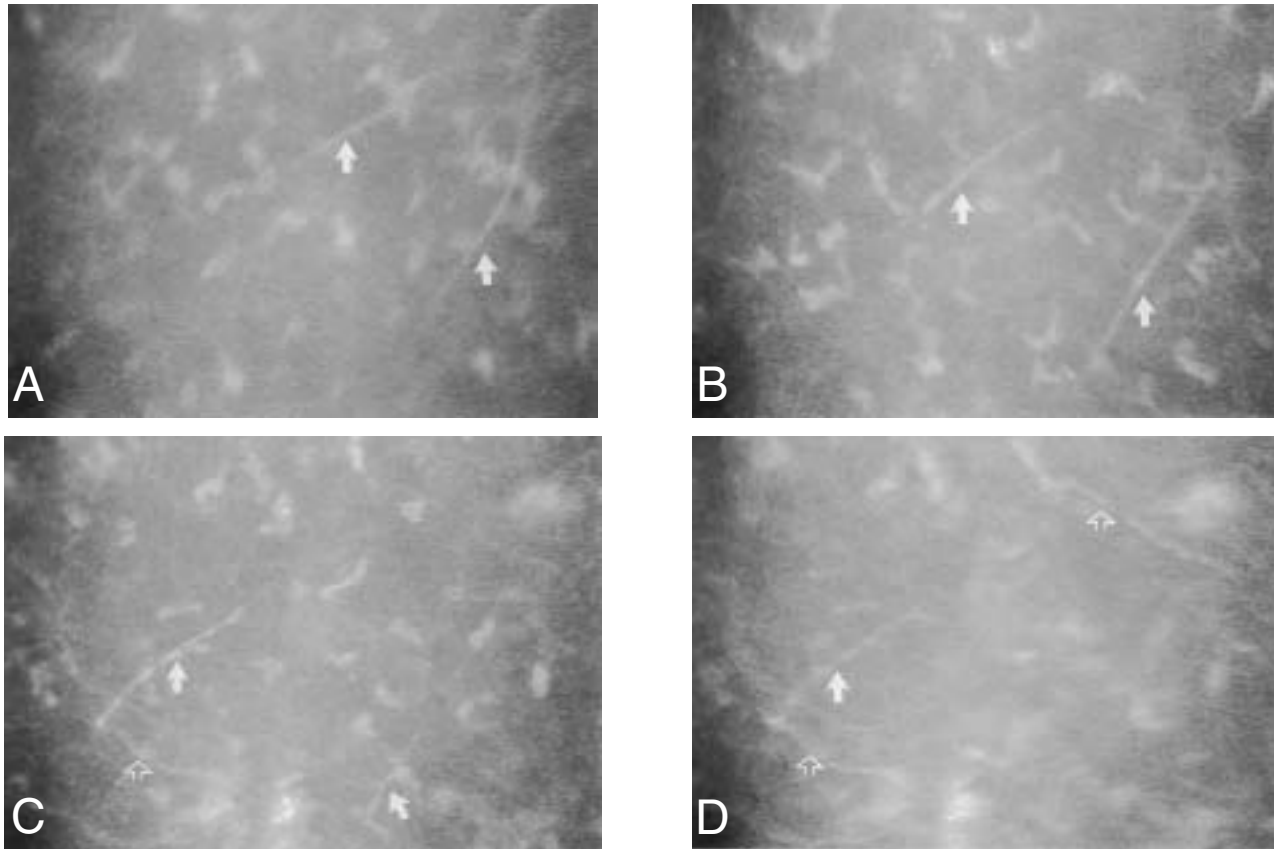
FIGURE 19

Regenerating anterior stromal nerves rise to directly reinnervate the post-PRK subbasal nerve plexus at 24 months. A, Two stromal nerves at 38 µm deep to the subbasal plexus (arrows). B, The 2 stromal nerves rise 21 µm through the anterior stroma (arrows). C and D, The stromal nerves (solid arrows) directly innervate obliquely oriented subbasal nerve fiber bundles (open arrows) found among keratocytes just posterior to the epithelium.
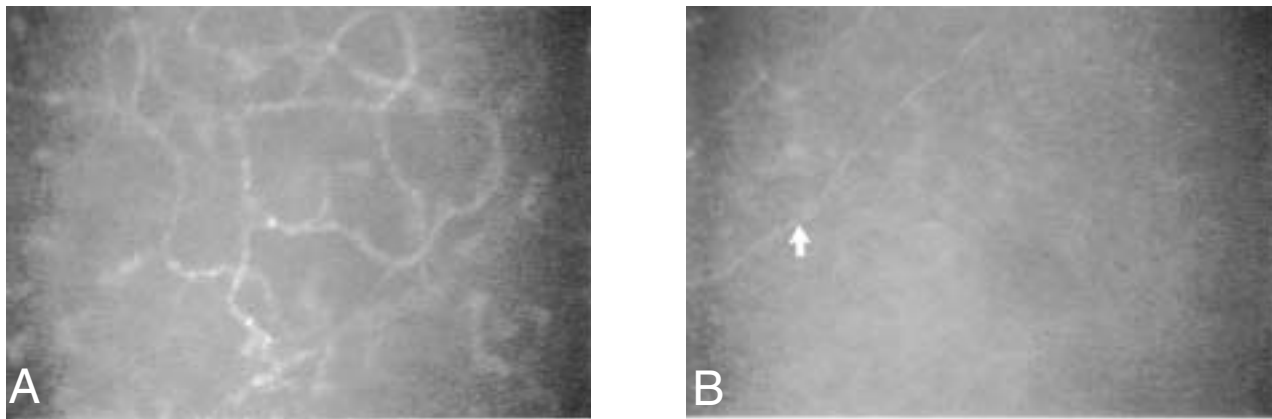

FIGURE 20

A, Confocal image of aberrant anterior stromal nerves identified 12 months after a reoperation to correct a regression of −1.00 D (initial PRK performed 13 months before the reoperation). B, Stromal nerve at the same adjusted stromal depth in the same subject before the reoperation (*arrow*).

to smooth out irregularities on the corneal surface.

Reinstein and colleagues[42] suggested that the origin of epithelial remodeling might be the semirigid, concave tarsus of the upper eyelid, which polishes and remodels the epithelial surface during blinking. A mechanical influence of the upper eyelid on a flatter cornea after PRK may result in postoperative epithelial thickening. The current data confirmed previous studies[192,195] that greater epithelial thickening was associated with deeper stromal ablation depths. The data also showed no association between postoperative epithelial thickening and subbasal nerve regeneration, the presence of activated keratocytes, or postoperative haze. No studies, however, have investigated the effect of a flatter cornea on epithelial thickness in normal corneas.
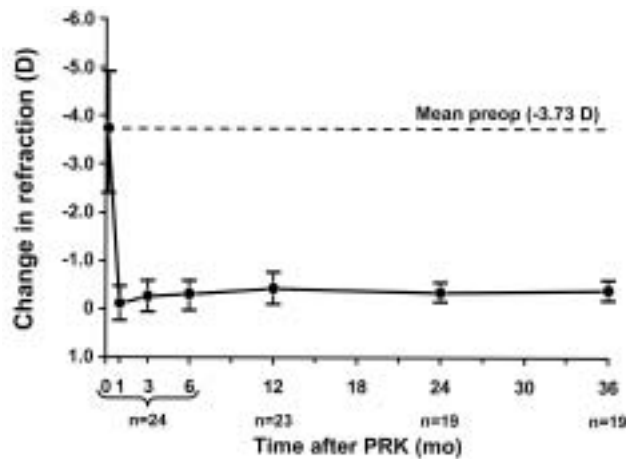
FIGURE 21

Change in refraction (mean ± SD) after PRK.

The 21% increase in central epithelial thickness documented in the first 12 months after PRK in the current study is similar to the 22% increase in epithelial thickness reported by Erie and colleagues[45] in the first 12 months after LASIK. The two procedures, however, differ in the amount of time required to establish a stable epithelial thickness. In the current PRK study, the epithelium required 12 months to establish a stable thickness, whereas after LASIK, epithelial thickness stabilized in only 1 month.[84] Wilson and colleagues[126] showed that the proliferation and differentiation of the healing epithelium are regulated by cytokines produced by activated keratocytes. Activated keratocytes in the current PRK study were located immediately beneath the epithelium and occupied a narrow region of anterior stroma (23 ± 10 µm). Keratocytes remained activated for up to 6 months after PRK. In contrast, after LASIK, activated keratocytes are not located in the anterior stroma but in the mid-stroma (160 ± 28 µm), immediately adjacent to the ablation interface. Similar to PRK, activated keratocytes occupy a narrow region of stroma (23 ± 13 µm), but unlike PRK, they are present for only a short time (1 to 4 weeks post-LASIK).[84] The time required to establish a stable epithelial thickness after PRK may be prolonged compared to LASIK because of the complex interaction between epithelial cells and activated keratocytes, which are present longer and are located closer to the epithelium after PRK than after LASIK.

Many investigators[123,194,200,201] have demonstrated epithelial thickening to be an important factor in myopic regression after PRK, although one study[110] did not find an association. The current data showed a significant correlation between epithelial thickening and myopic regression. At 1 year after PRK, a 12-µm increase in epithelial thickness was associated with a myopic regression of –0.41 D. The fundamental PRK treatment algorithm of Munnerlyn

and associates[202] predicts a 13-µm central tissue photoablation per diopter of refractive power change (6.0 mm diameter PRK). Thus, if postoperative epithelial thickening was limited to the central photoablation zone, the observed increase in central epithelial thickness was 2.6-fold greater than would be predicted for the degree of myopic regression that was observed. This suggests that postoperative epithelial thickening in the peripheral ablation zone may partially negate the steepening and subsequent myopic effect of central epithelial thickening. More extensive confocal microscopy examination of the peripheral ablation zone is needed to analyze potential differences between central and peripheral epithelial thickening.

Because the thickness of the regenerated epithelium did not stabilize until 1 year after PRK and because it was correlated with myopic regression, it seems reasonable to defer any further treatment of myopic regression until 1 year after the original PRK. This allows adequate time for the regenerated epithelium to stabilize at its maximum thickness and to reach its full refractive effect.

STROMAL THICKNESS

The corneal stroma is unique in its composition and the precise organization of the stromal ECM. In humans, the corneal stroma undergoes homeostatic remodeling at a considerably slower rate than the dermis of the skin or most other collagenous tissues.[56] Davison and Galbavy[203] showed that there is no detectable turnover of stromal ECM in the unwounded human cornea during many months follow-up.

The current study attempted to quantify stromal thickening between 1 and 36 months after corneal wounding by PRK. After PRK in rabbits, histologic[123,163,164,191] and confocal microscopy[95,162] studies have demonstrated that the corneal stroma possesses the ability to thicken dramatically. After PRK in primates and humans, histologic studies[87,90,165,167,169-172] have identified, but not quantified, the presence of newly secreted ECM, although in much lesser amounts than that observed in the highly reactive rabbit. A recent confocal microscopy in vivo study documented a small stromal regrowth of 6 µm between 1 and 12 months after PRK in humans.[110] The investigators suggested that the deposition of new ECM was the main repair mechanism by which the human stroma gradually regained thickness and curvature after PRK.

The current study found no significant increase in stromal thickness at any time after PRK compared with the stromal thickness at 1 month post-PRK. In addition, stromal thickening was not correlated with myopic regression. After PRK, anterior stromal keratocytes become activated to repair-fibrocytes.[160] Much of the synthetic activity of the repair-fibrocytes is involved with the production of repair ECM.[86,157,158] However, repair-fibro-

cytes not only synthesize new ECM but also turn on new synthesis of enzymes that can degrade ECM.[86] Cionni and colleagues[204] have shown that the new ECM of the repair tissue is actively remodeled over months by continual synthesis, degradation, and resynthesis of collagens and other ECM components. Remodeling of stroma by continual synthesis and degradation may explain why the current study found no significant increase in stromal thickness. Although the change in stromal thickness was not significant and not correlated with myopic regression, the combined effect of epithelial and stromal thickening (corneal thickening) was complementary and was strongly correlated with myopic regression.

KERATOCYTE DENSITY

The first part of the current study compared the keratocyte density in the post-PRK stroma to the cell density in the pre-PRK full stroma (pre-PRK stromal thickness not adjusted for ablation depth, Figure 5). Keratocyte density is highest in the most anterior stroma of the normal human cornea.[58-60] The dense keratocyte population found in the preoperative anterior stroma was partially or completely removed during PRK excimer photoablation, and this high keratocyte density was not reconstituted in the post-PRK anterior stroma. This observation has not been described previously in humans after PRK. Specifically, keratocyte density in the anterior 0% to 10% stroma was reduced 40%, 43%, and 45% at 12, 24 and 36 months post-PRK compared with the anterior 0% to 10% of the pre-PRK full stroma. Because of this significant reduction in the anterior keratocyte population, the keratocyte density in the full-thickness stroma was 11% lower at 36 months after PRK than preoperatively. In addition, the distribution of keratocytes throughout the post-PRK stroma was altered such that keratocytes in the post-PRK stroma were distributed uniformly throughout the anterior-posterior stroma (Figure 11) This is in contrast to the normal human stroma, in which keratocytes are distributed nonuniformly throughout the anterior-posterior stroma, with a much greater cell density anteriorly (Figure 3, Figure 11).

What a depleted anterior stromal keratocyte population after PRK means for the long-term health of the human cornea is unknown. There may be no need to replace keratocytes to the high density found in the preoperative anterior stroma. It has been hypothesized, however, that a keratocyte-rich anterior stroma represents some form of protection against infection of the corneal epithelium, minimizing posterior extension of the infection.[160] In addition, a reduced keratocyte density has been observed in the anterior stroma of contact lens wearers with the ectatic corneal dystrophy keratoconus.[73] Thus, the wound healing response to subsequent trauma or infection, the influence of mediators released from the epithelium, the absence of Bowman's membrane, and the continued effect of time on an altered keratocyte distribution are yet to be determined. The clinical importance of the current study's observed keratocyte density changes will be appreciated only after longer follow-up.

Apoptotic keratocyte loss immediately after PRK or epithelial scrape injury resulting in an acellular region of anterior stroma has been well documented in rabbit studies.[137,141,147,161] Recently, Ambrosio and colleagues[205] confirmed that human keratocytes undergo apoptosis in response to epithelial debridement in a manner similar to rabbits. In a human histologic study, Balestrazzi and colleagues[170] measured a 5 to 8 µm region of acellular anterior stroma at 3 months after PRK.

The tandem scanning confocal microscope is not capable of detecting a completely acellular region of anterior stroma early after PRK when landmarks such as the epithelium and subbasal plexus have not yet re-formed.[51] Therefore, the current study cannot address the presence or absence of a zone of acellular anterior stroma immediately after PRK. However, the current study did demonstrate a significant reduction in keratocyte density in the most anterior confocal image compared with the next-deeper analyzed confocal image (5% to 10% stromal depth) at 5 days after PRK. This difference in keratocyte density would not be expected in the normal cornea and was not observed at other examinations after PRK, including 1 day post-PRK. This measured decrease in keratocyte density in the most anterior confocal image 5 days after PRK may represent the apoptotic cell loss demonstrated in humans by Ambrosio and colleagues.[205] Increased light scatter from the contact lens present at 5 days may also have obscured the most anterior keratocytes.

The extent of apoptotic cell death after PRK has been associated with the method of epithelial removal. Transepithelial PRK has been shown to result in comparatively low levels of keratocyte apoptosis.[88,161] The laser-scrape technique, used in the current study, is a method of epithelial removal that is similar to transepithelial ablation. It is possible that laser-scrape epithelial removal also decreases the degree of keratocyte apoptosis, resulting in a reduction but not a complete loss of superficial keratocytes. Irrigation with cold balanced salt solution may also affect keratocyte apoptosis in the retroablation zone.

The initial apoptotic keratocyte loss after PRK triggers a subsequent proliferation of keratocytes.[132,133,142,160] In the highly reactive rabbit, the volume void of keratocytes is repopulated within a few days after surgery.[159-161] In the second part of the current study, keratocyte density in the post-PRK stroma was compared with keratocyte density in the pre-PRK future unablated stroma. In the pre-PRK

future unablated stroma, the thickness of anterior stroma destined to be photoablated was omitted from the analysis. This allowed a direct comparison of keratocyte density in the same tissue layers in the pre- and post-PRK stroma (Figure 5). The current data confirm previous primate[85,165,167,169] and human[51,54,85,95,171,172,205] studies that demonstrated an initial proliferation of keratocytes in the anterior stroma at 1 month after PRK that becomes maximal by 3 months compared with the same tissue layer of the preoperative stroma. It has been hypothesized that the increase in cell density in humans occurs by keratocyte migration or by keratocyte mitosis, which has been demonstrated in animal models after corneal freeze injuries,[206] after destruction of stromal keratocytes by mustard and nitrogen mustard gases,[207] and after epithelial scraping.[137,142,143]

A new observation at 3 months post-PRK was an increased keratocyte density in the middle and posterior stroma in addition to an increased cell density in the anterior stroma. This suggests that PRK can influence the proliferation and migration of keratocytes throughout the full-thickness corneal stroma. It is not known why laser ablation at the corneal surface would affect keratocyte density in the middle and posterior stroma. Endothelial cell density is not affected by PRK.[208] Several investigators, however, have provided evidence for a functional, elaborate, 3-dimensional keratocyte network that implies lateral and anterior-posterior communication.[59,86,209] Cell:cell attachment is mediated by long cellular processes creating a continuous syncytium. Freeze fracture and dye transfer studies reveal that keratocytes are joined by gap junctions within which small molecules diffuse freely.[210] The presence of an anterior-posterior communication network between keratocytes may, in part, explain the effect of surface excimer ablation on keratocytes deeper in the stroma.

Consistent with previous confocal studies,[54,85,95] the current study confirmed that keratocyte density in the same tissue layers returned to preoperative levels by 6 months after PRK. In dermal wounds this return to normal cell density has been shown to occur by apoptosis,[211] and it is thought that the same process may occur in corneal wounds.[86,160] The long-term effect of PRK on keratocyte density has not previously been known. New long-term data provided by the current study demonstrate that keratocyte density in the anterior 10% of the post-PRK stroma continues to decrease approximately 5% per year between 1 and 3 years after surgery compared with the same tissue layer preoperatively (Figure 14). The progressive decline in the anterior stroma keratocytes became statistically significant at 36 months after PRK (P = .02). In contrast, keratocyte density in the middle and posterior stroma remained unchanged between 1 and 3 years after PRK compared with preoperative values. The reason for

the observed progressive decline in the anterior keratocyte population is not known. Fini[86] hypothesized that this also represents continued apoptotic cell loss rather than cell necrosis. Alternatively, Vesaluoma and colleagues[212] suggested that denervation may play a role in the diminished density of keratocytes. Mitooka and colleagues[84] noted a similarity between reinnervation of the cornea and recovery of keratocyte density after LASIK. Muller and colleagues[49] demonstrated the direct innervation of individual keratocytes. The lack of a trophic factor that would normally be supplied by nerves could affect the most anterior keratocytes and decrease their density. The data from the current study, however, do not support this hypothesis because no association between corneal reinnervation and keratocyte density was found at any time after PRK.

Interpretation of keratocyte density measurements made by using confocal microscopy has some limitations. First, stromal edema present at 1 and 5 days post-PRK could falsely decrease keratocyte density. However, the anterior 100 to 120 µm of human corneal stroma does not swell perceptibly; swelling is confined mainly to the posterior stroma.[213,214] Muller and colleagues[213] elegantly demonstrated how the stromal interweave architecture of the anterior stroma is resistant to swelling. Therefore, any differences in cell density between the most anterior confocal image and the next deeper image (5% to 10% stromal depth) because of differential swelling should be minimal. However, the stromal swelling present at 1 and 5 days after PRK (but not thereafter) would have decreased the measured cell density in the middle and posterior layers and should be considered when interpreting these cell densities. Second, inflammatory cells have been seen in histologic studies during the first week after PRK in the highly reactive rabbit cornea[3,215] and to a lesser degree in the primate cornea.[87] Some of the cell nuclei that were counted during the first week after PRK may have been clusters of inflammatory cells, and this would artificially increase the measured keratocyte density.

KERATOCYTE MORPHOLOGY AND CORNEAL HAZE

Classic studies describe changes in keratocyte morphology after surgical incision into the mammalian cornea.[216-218] Keratocytes adjacent to the wound disappear by apoptosis within a few hours of surgery.[147] The process of repair in the corneal stroma begins with the activation or transformation of quiescent keratocytes into repair-fibrocytes adjacent to the acellular zone.[86,156,157] Histologically, the first detectable morphologic changes associated with an actively synthetic repair-fibrocyte are an increase in cell size, an increase in the size and number of nucleoli, many rough endoplasmic reticula, mitochondria, free ribosomes, and Golgi complexes.[86] With the confocal microscope, activated keratocyte or repair-fibrocyte nuclei are

identified by a large, brightly reflective appearance associated with visible cytoplasmic processes.[47,81,84,85,88]

The current study provided new confocal microscopy data that keratocytes at 1 day after PRK were morphologically unchanged compared with preoperative quiescent keratocytes. No previous confocal microscopy studies have examined corneas as early as 1 day after PRK. Beginning at 5 days after PRK, confocal microscopy evidence of activated keratocytes or repair-fibrocytes first appeared. The number of corneas with activated keratocytes or repair-fibrocytes peaked at 3 months, and activated keratocytes were no longer visible in any corneas by 12 months after PRK. These findings are consistent with previous human histologic[170-172] and confocal microscopy[51,54,85,95] studies that have documented the presence of activated anterior keratocytes in the first 3 weeks to 4 months after PRK.

In the first 3 months after PRK, activated keratocytes were found to occupy a very narrow zone of 23 ± 10 µm (range, 10-57 µm) in the most anterior stroma immediately beneath the epithelium. The depth of stromal involvement by activated keratocytes after PRK has not been quantified previously in vivo. Taylor and colleagues,[171] in a human histologic study, described activated keratocytes in a 10- to 15-µm thick zone directly underlying the epithelium at 4 months after PRK. After LASIK, the zone of activated keratocytes posterior to the ablation interface (23 ± 13 µm) is identical in size to that observed in the current PRK study.[84]

Activated keratocytes or repair-fibrocytes are involved in the production of repair ECM.[157,158] Post-PRK corneal haze (backscattered light) has been attributed to changes in the repair ECM and changes in the individual activated keratocytes.[110,158] The current study was unable to differentiate between backscattered light from the cells (activated keratocytes) and backscattered light from the background (repair ECM). Similar to previous studies, the current study showed that confocal microscopy haze estimates were associated with ablation depth[120,165,171] and myopic regression.[219]

CORNEAL NERVE MORPHOLOGY AND DENSITY
Quantification of nerve density has been attempted in the central corneas of normal subjects by using the scanning slit confocal microscope[59,60] and after LASIK using the tandem scanning confocal microscope.[101] Oliveira-Soto and Efron,[59] using the scanning slit confocal microscope, found the central subbasal nerve density to be 826 ± 319 µm within an area of 0.074 mm² (frame size, 0.315 × 0.236 mm) or 11,111 µm/mm². The current study, using the tandem scanning confocal microscope, determined the central subbasal nerve density in the preoperative normal cornea to be 6,944 µm/mm². There are two factors that

likely account for this difference. First, Oliveira-Soto and Efron[59] selected the "most representative" image for analysis so that selection bias may have played a role. The current study used a sampling technique that evaluated all scans of sufficient quality to visualize nerves (3 to 8 scans per eye). Second, the higher light throughput from the scanning slit confocal microscope may improve the signal-to-noise ratio and contrast and provide an improved image compared to tandem scanning. Therefore, density values in the two systems may not be directly comparable. Because individual nerve fibers are not seen by any type of confocal microscope, the nerve densities reported by confocal microscopy cannot be translated directly to histologic studies of neurophysiologic function.

Quantification of nerve density has not been attempted previously in humans after PRK. In the current study, corneal nerves before and after PRK were divided into two groups: subbasal nerve fiber bundles and stromal nerve fiber bundles. Subbasal nerve fiber bundles were first visualized in 17% of the corneas at 1 month after PRK, but at a density that was 98% less than preoperative density. The lack of visible subbasal nerves this early after PRK may be because the nerve plexus was either reduced or absent or the hyperreflectivity of the subepithelial stroma and the lack of a dark Bowman's membrane masked the visibility of fine nerves. Subsequently, subbasal nerve density was still reduced 87%, 75%, and 60% at 3, 6, and 12 months after PRK before eventually returning to levels at 24 and 36 months after PRK that were not statistically different from values before PRK. However, the current study could not exclude, with 80% certainty, the possibility that nerve density was still decreased by 30% 36 months after PRK. The current quantitative data confirm earlier qualitative human PRK data that the subepithelial plexus is reduced early after PRK and remains abnormal at 1 year.[85,95] Rabbit PRK data, which may be comparable to humans, showed that regenerated subepithelial nerves regain normal density and architecture at 1 year.[97] After LASIK in humans, Lee and colleagues[101] found that, similar to PRK, the number of subbasal nerve fiber bundles was reduced 50% at 1 year. No additional quantitative studies with longer follow-up after LASIK are available.

Along with a change in nerve density, the regenerating subbasal nerve fiber bundles in the central cornea also demonstrated a change in nerve orientation. In the first 6 months after PRK, the central subbasal nerves were arranged in a horizontal or oblique orientation. Between 6 and 12 months after PRK, the subbasal nerve orientation rotated and returned to the relatively vertical orientation found in the normal preoperative central subbasal nerve plexus. This observation has not been reported in humans after PRK. However, a similar neural rotational remodeling has been observed in the rabbit after dener-

vation.[186] The reason for a change in central subbasal nerve orientation is not known but suggests an ongoing reorganization process.

The second group of corneal nerves studied was the stromal nerve fiber bundles. The number of central stromal nerve fiber bundles in the current study was unchanged up to 36 months after PRK compared with the preoperative number. However, a morphologic change was observed in the architecture of the regenerated anterior stromal nerves. Similar to neural remodeling in the rabbit,[97,185,186] regenerating anterior stromal nerve trunks rose to the most anterior stroma and supplied new subbasal nerve fiber bundles (Figure 23). This neural reorganization was first identified in some corneas at 6 months after PRK. The number of corneas with this pattern of neural remodeling increased over time, but it was observed in only 63% of the eyes at 36 months after PRK, suggesting that the remodeling process was still incomplete.

Apparently, errors may occur in stromal nerve regeneration. Aberrant stromal nerve regeneration has been reported after LASIK but not after PRK.[220] In the current study, aberrant anterior stromal nerves with a coiled course and irregular branching pattern were identified 1 year after PRK reoperation. The abnormal stromal nerve pattern persisted for 2 years after the PRK reoperation. The reason for aberrant regeneration is unclear. PRK and LASIK always sever stromal nerves. Subsequent nerve regrowth may be the function of some peripheral target. Neuronotrophic action of the target tissue on regenerating nerves has been demonstrated in the skin of rats and in motor end-plates.[221] Moreover, some studies indicate that in the case of the cornea, epithelial cells release factors that stimulate trigeminal neurons to form neurites.[222] Although by confocal microscopy the aberrant stromal fibers seemed to end blindly in the stroma and the subbasal nerve fiber bundle density was decreased objectively, corneal sensation was normal as tested by using Cochet-Bonnet esthesiometry.

There is a discrepancy between the reported density of subbasal nerve fiber bundles and the measurement of corneal sensitivity. After PRK, most investigators have shown that the recovery of corneal sensitivity, as tested by Cochet-Bonnet esthesiometry, occurs in 4 to 6 weeks and is complete within 6 to 12 months after surgery.[103, 223-225] Kanellopoulos and colleagues,[226] in contrast, showed that corneal sensitivity was still abnormal 12 months after PRK. Murphy and colleagues[227] showed that the reduction of corneal sensitivity was not related to the depth of PRK ablation. In the current study, corneal sensitivity, as measured by Cochet-Bonnet esthesiometry, was normal at 12 months after PRK even when the subbasal nerve fiber bundle density was reduced by 60% (corneal sensitivity was not tested less than 12 months after PRK). Many factors may account for this difference. First, confocal microscopy cannot visualize the epithelial axon terminals originating from the subbasal nerve plexus. Second, increased backscatter of light (haze) at the stromal interface reduces contrast and may decrease the visibility of fine nerves, resulting in a falsely low density. Third, too little light scatter by the newly regenerated nerves may contribute to reduced detection when using tandem scanning confocal microscope. Fourth, the Cochet-Bonnet method is limited in that it detects neurons sensitive to mechanical stimulation only. Use of noncontact gas esthesiometry, which discriminates between the three classes of nociceptors in the cornea—mechanosensory, polymodal, and cold-sensory neurons—may better detect the presence or absence of altered corneal sensation.[228]

SUMMARY

1. The central corneal epithelium thickens 21% in the first year after PRK. The increased epithelial thickness stabilizes by 1 year after PRK but does not return to pre-PRK thickness by 3 years.

2. The central corneal stromal thickness remains stable after PRK and does not significantly change between 1 and 36 months after PRK.

3. The dense keratocyte population found in the preoperative anterior stroma is partially or completely removed during PRK photoablation. This high keratocyte density is not reconstituted in the anterior 10% of the post-PRK stroma and results in a new uniform distribution of keratocytes throughout the anterior-posterior post-PRK stroma. Specifically, keratocyte density is reduced 43% in the anterior 10% of the post-PRK stroma at 36 months compared with the density in the anterior 10% of the pre-PRK full stroma (stromal thickness not adjusted for ablation depth).

4. Adjusting the pre-PRK stromal thickness for the thickness of stroma destined to be photoablated allows for a direct comparison of the same tissue layers in the pre- and post-PRK stroma. Doing this demonstrates an initial increase in keratocyte density throughout the full-thickness stroma by 3 months after PRK before returning to preoperative densities by 6 months after PRK. Subsequently, there is a progressive decline in keratocyte density in the anterior 10% of the post-PRK stroma that becomes statistically significant by 3 years.

5. After PRK, activated keratocytes or repair-fibrocytes are first identified by confocal microscopy at 5 days after PRK, peak at 3 months after PRK, and are last seen at 6 months after PRK. Activated keratocytes occupy a narrow zone (23 ± 10 µm) in the anterior stroma immediately posterior to the epithelium.

6. Corneal subbasal nerves that are lost immediately

after PRK gradually return; however, the recovery of subbasal nerve density is less than half complete by 12 months after PRK. Specifically, subbasal nerve fiber bundle density is reduced 98%, 87%, 75%, and 60% at 1, 3, 6, and 12 months after PRK. At 24 and 36 months after PRK, subbasal nerve fiber bundles are still subjectively thinner than preoperative but their density has returned to levels that are not significantly different from preoperative. The regenerated central subbasal nerve fiber bundles demonstrate a mean horizontal orientation in the first 6 months after PRK before returning to their preoperative vertical orientation by 12 months after PRK.

7. Regenerating anterior stromal nerves demonstrate a morphologic change in their architecture after PRK. Beginning at 6 months after PRK, regenerating stromal nerve trunks are seen to rise to the most anterior stroma and directly supply new subbasal nerve fiber bundles. This pattern of neural reorganization, though still incomplete at 36 months, suggests that human stromal nerves regenerate after PRK in a manner similar to rabbits. In addition, aberrent regeneration of anterior stromal nerves may occur after PRK reoperations.

8. Myopic regression occurs in 78% of eyes in the first year after PRK and is significantly correlated with epithelial thickening, corneal thickening, and confocal microscopy corneal haze estimates.

ACKNOWLEDGMENT

REFERENCES

1. Drews RC. The role of the iris in the healing of corneal wounds. *Trans Am Opthalmol Soc* 1979;77:422-463.
2. Koch DD. Histological changes and wound healing response following noncontact holmium:YAG laser thermal keratoplasty. *Trans Am Ophthalmol Soc* 1996;94:745-802.
3. Steinert RF. Wound healing anomalies after excimer laser photorefractive keratectomy: correlation of clinical outcomes, corneal topography, and confocal microscopy. *Trans Am Ophthalmol Soc* 1997;95:629-714.
4. Trokel SL, Srinivasan R, Braren B. Excimer laser surgery of the cornea. *Am J Ophthlamol* 1983;96:710-715.
5. Goldman H. Spaltlampenphotographie und -photometrie. *Ophthalmologica* 1940;98(5/6):257-270.
6. Minsky M. Memoir on inventing the confocal scanning microscope. *Scanning* 1988;10:128-138.
7. Minsky M. Microscopy apparatus. US patent 3,013,467. Dec 19, 1961.
8. Petran M, Hadravsky M, Eggar MD, et al. Tandem-scanning reflected light microscope. *J Opt Soc Am* 1968;58:661-664.
9. Petran M, Hadravsky M, Kucera BR. The tandem scanning reflected light microscope. *Proc R Microscop Soc* 1985;20:125-129.
10. Nipkow P. German patent No. 30105, published January 15, 1884.
11. Eggar MD, Petran M. New reflected-light microscope for viewing unstained brain and ganglion cells. *Science* 1967;157:305-307.
12. Eggar MD, Gerazi W, Davidovitz P, et al. Observations of nerve fibers in incident light. *Experientia* 1969;25:1125.
13. Lemp MA, Dilly PN, Boyde A. Tandem-scanning (confocal) microscopy of the full-thickness cornea. *Cornea* 1985/1986;4:205-209.
14. Jester JV, Andrews PM, Petroll WM, et al. In vivo, real-time confocal imaging. *J Electron Microsc Tech* 1991;18:50-60.
15. Jester JV, Petroll WM, Garana RMR, et al. Comparison of in vivo and ex vivo cellular structure in rabbit eyes detected by tandem scanning microscopy. *J Microsc* 1991;165:169-181.
16. Petroll WM, Cavanagh HD, Lemp MA, et al. Digital image acquisition in in vivo confocal microscopy. *J Microscop* 1991;165:61-69.
17. Cavanagh HD, Jester JV, Essepian J, et al. Confocal microscopy of the living eye. *CLAO J* 1990;16:65-73.
18. Masters BR. *Noninvasive Diagnostic Techniques in Ophthalmology*. New York: Springer-Verlag; 1990.
19. Patel SV, McLaren JW, Camp JJ, et al. Automated quantification of keratocyte density by using confocal microscopy in vivo. *Invest Ophthalmol Vis Sci* 1999;40:320-326.
20. Svishchev GM. Microscope for the study of transparent light-scattering objects in incident light. *Opt Spectrosc* 1969;26:171-172.
21. Svishchev GM. Image contrast in a microscope with synchronous scanning of the object by point and raster field diaphragms. *Opt Spectrosc* 1973;34:221-224.
22. Baer SC. Optical apparatus providing focal-plane-specific illumination. US patent 3,547,512. June 30, 1970.
23. Baer SC. Tandem scanning slit microscope. *Opt Stor Scan Tech* 1989;1139:99-101.
24. Maurice DM. A scanning slit optical microscope. *Ophthalmology* 1974;13:1033-1037.
25. Koester CJ, Roberts CW, Donn A, et al. Widefield specular microscopy: clinical and research applications. *Ophthalmology* 1980;87:849-855.
26. Thaer AA, Geyer OC, Kaszli FA. Fluorogenic substrate techniques applied to the noninvasive diagnosis of the living rabbit and human cornea. In Masters BR, ed: *Noninvasive Diagnostic Techniques in Ophthalmology*. New York: Springer-Verlag; 1990:569-590.
27. Masters BR, Thaer AA. Real-time scanning slit confocal microscopy of the *in vivo* human cornea. *Appl Opt* 1994;33:695-701.

28. Masters BR, Thaer AA. In vivo, real-time confocal microscopy of the continuous wing cell layer adjacent to the basal epithelium in the human cornea: a new benchmark for in vivo corneal microscopy. *Bioimages* 1995;3:7-11.

29. Masters BR. *Selected Papers on Confocal Microscopy.* Bellingham, Wash: Bellingham, Wash: International Society for Optical Engineering; 1996. SPIE milestone series v MS131.

30. Wilson T. *Confocal Microscopy*. London: Academic Press; 1990.

31. Masters BR. Design considerations of a real-time clinical confocal ophthalmoscope. In: Puliafito, CA, ed. *Ophthalmic Technologies*. *Proc SPIE*. 1991;1423:8-14.

32. Masters BR. Scanning microscope for optically sectioning the living cornea. In: Wilson T, ed. *Scanning Imaging. Proc SPIE*. 1989;1028:133-143.

33. Xiao GQ, Corle TR, Kino GS. Real-time confocal scanning optical microscope. *Appl Phys Lett* 1988;53:716-718.

34. Xiao GQ, Kino GS, Masters BR. Observations of the rabbit cornea and lens with a new real-time confocal scaning optical microscope. *Scanning* 1990;12:161-166.

35. Tomii S, Kinoshita S. Observations of human corneal epithelium by tandem scanning confocal microscope. *Scanning* 1994;16:305-306.

36. Mustonen RK, McDonald MB, Srivannaboon S, et al. Normal human corneal cell populations evaluated by in vivo scanning slit confocal microscopy. *Cornea* 1998;17:485-492.

37. McCally RL, Farrell RA. Light scattering from cornea and corneal transparency. In: Masters BR, ed. *Noninvasive Diagnostic Techniques in Ophthalmology*. New York: Springer-Verlag; 1990:189-210.

38. Calmettes L, Deodati F, Planel H, et al. Etude Histologique et Histochimique de L'epithelium Anterieur. *Arch Ophthalmol (Paris)* 1956;16:481-506.

39. Ehlers N. The epithelial surface. *Acta Ophthalmol (Copenh)* 1965;43(suppl 181):35-54.

40. Wolff E. The anatomy of the eye and orbit. In: Bron AJ, ed. *Anatomy of the Eye and Orbit*. Philadelphia: WB Saunders; 1997:34

41. Reinstein DZ, Silverman RH, Rondeau MJ, et al. Epithelial and corneal thickness measurements by high-frequency ultrasound digital signal processing. *Ophthalmology* 1994;101:140-146.

42. Reinstein DZ, Silverman RH, Sutton HFS, et al. Very high frequency ultrasound corneal analysis identifies anatomic correlates of optical complications of lamellar refractive surgery. Anatomic diagnosis in lamellar surgery. *Ophthalmology* 1999;106:474-482.

43. Li HF, Petroll WM, Moller-Pedersen T, et al. Epithelial and corneal thickness measurements by in vivo confocal microscopy through focusing (CMTF). *Curr Eye Res* 1997;16:214-221.

44. Patel SV, McLaren JW, Hodge DO, et al. Normal human keratocyte density and corneal thickness measurements by using confocal microscopy in vivo. *Invest Ophthlamol Vis Sci* 2001;42:333-339.

45. Erie JC, Patel SV, McLaren JW, et al. The effect of myopic laser in situ keratomileusis on epithelial and stromal thickness. *Ophthalmology* 2002;109:1447-1452.

46. Prydal JI, Kerr Muir MG, Dilly PN, et al. Confocal microscopy using oblique sections for measurement of corneal epithelial thickness in conscious humans. *Acta Ophthalmol Scand* 1997;75:624-628.

47. Moller-Pedersen T, Vogl M, Li HF, et al. Quantification of stromal thinning, epithelial thickness, and corneal haze after photorefractive keratectomy using in vivo confocal microscopy. *Ophthalmology* 1997;104:360-368.

48. Kauffmann T, Bodanowitz S, Horle S. In vivo study of basal cell density in healthy human eyes and after PRK using a confocal videomicroscope. *Invest Ophthalmol Vis Sci* 1996;37(ARVO suppl):3.

49. Muller LJ, Pels L, Vrensen GFJM. Ultrastructural organization of human corneal nerves. *Invest Ophthalmol Vis Sci* 1996;37:476-488.

50. Muller LJ, Vrensen GFJM, Pels L, et al. Architecture of human corneal nerves. *Invest Ophthalmol Vis Sci* 1997;38:985-994.

51. Erie JC, Patel SV, McLaren JW, et al. Keratocyte density in vivo after photorefractive keratectomy in humans. *Trans Am Ophthalmol Soc* 1999;97:221-240.

52. Prydal JI, Franc F, Dilly PN, et al. Keratocyte density and size in conscious humans by digital image analysis of confocal images. *Eye* 1998;12:337-342.

53. Berlau J, Becker H-H, Stave J, et al. Depth and age-dependent distribution of keratocytes in healthy human corneas. *J Cataract Refract Surg* 2002;28:611-616.

54. Frueh BE, Cadez R, Bonke M. In vivo confocal microscopy after photorefractive keratectomy in humans. A prospective, long-term study. *Arch Ophthalmol* 1998;116:1425-1431.

55. Poole CA, Brookes NH, Clover GM. Keratocyte networks visualized in the living cornea using vital dyes. *J Cell Sci* 1993;106:685-692.

56. Muller LJ, Pels L, Vrensen GF. The novel aspects of the ultrastructural organization of human corneal keratocytes. *Invest Ophthalmol Vis Sci* 1995;36:2557-2567.

57. Moller-Pedersen T, Ehlers N. A three-dimensional study of the human corneal keratocyte density. *Curr Eye Res* 1995;14:459-464.

58. Patel SV, McLaren JW, Camp JJ, et al. Automated quantification of keratocyte density by using confocal microscopy in vivo. *Invest Ophthalmol Vis Sci* 1999;40:320-326.

59. Oliveira-Soto L, Efron N. Morphology of corneal nerves using confocal microscopy. *Cornea* 2001;20:373-384.

60. Grupcheva CN, Wong T, Riley AF, et al. Assessing the subbasal nerve plexus of the living healthy human cornea by in vivo confocal microscopy. *Clin Experiment Ophthalmol* 2002;30:187-190.

61. Salz JJ, Azen SP, Berstein J, et al. Evaluation and comparison of sources of variability in the measurement of corneal thickness with ultrasonic and optical pachymeters. *Opthalmic Surg* 1983;14:750-754.

62. Reader III AL, Salz JJ. Differences among ultrasonic pachymeters in measuring corneal thickness. *J Refract Surg* 1987;3:7-11.

63. Nissen J, Hjortdal JO, Ehlers N, et al. A clinical comparison of optical and ultrasonic pachymetry. *Acta Ophthalmol* 1991;69:659-663.

65. Modis Jr L, Langenbucher A, Seitz B. Scanning-slit and specular microscopic pachymetry in comparison with ultrasonic determination of corneal thickness. *Cornea* 2001;20:711-714.

64. Giasson C, Forthome D. Comparison of central corneal thickness measurements between optical and ultrasonic pachometers. *Optom Vis Sci* 1992;69:236-241.

66. Waring GO. Surgical instruments used in refractive keratotomy. In: Waring GO, ed. *Refractive Keratotomy*. St Louis: Mosby; 1992:407-431.

67. Edmund C. Determination of the corneal thickness profile by optical pachometry. *Acta Ophthalmol* 1987;65:147-152.

68. McLaren JW, Bourne WM. A new video pachometer. *Invest Ophthalmol Vis Sci* 1999;40:1593-1598.

69. Hitzenberger CK, Drexler W, Fercher AF. Measurement of corneal thickness by laser doppler interferometry. *Invest Ophthalmol Vis Sci* 1992;33:98-103.

70. Hitzengerger CK, Baumgartner A, Drexler W, et al. Interferometric measurement of corneal thickness with micrometer precision. *Am J Ophthalmol* 1994;118:468-476.

71. Maurice DM, Giardini AA. A simple optical apparatus for measuring the corneal thickness, and the average thickness of the human cornea. *Br J Ophthalmol* 1951;35:169-177.

72. Petroll WM, Cavanagh HD, Jester JV. Three-dimensional imaging of corneal cells using in vivo confocal microscopy. *J Microsc* 1993;170:213-219.

73. Erie JC, Patel SV, McLaren JW, et al. Keratocyte density in keratoconus. *Am J Ophthalmol* 2002;134:689-695.

74. Nau CB, McLaren JW, Lee BH, et al. Corneal thickness measurement: Disagreement between confocal microscopy and ultrasonic pachometry. *Invest Ophthalmol Vis Sci* [ARVO abstract] 2002;43:6.

75. McLaren JW, Nau CB, Patel SV, et al. How precisely can we determine keratocyte density by confocal microscopy? *Invest Ophthalmol Vis Sci* 2001;42:S281.

76. Cavanagh HD, Petrol WM, Alixadeth H, et al. Clinical and diagnostic use of in vivo confocal microscopy in patients with corneal disease. *Ophthalmology* 1993;100:1444-1454.

77. Moller-Pedersen T, Ledet T, Ehlers N. The keratocyte density of human donor corneas. *Curr Eye Res* 1994;13:163-169.

78. Moller-Pedersen T. A comparative study of human corneal keratocyte and endothelial cell density during aging. *Cornea* 1997;16:333-338.

79. Petroll WM, Boettcher K, Barry P, et al. Quantitative assessment of anteroposterior keratocyte density in the normal rabbit cornea. *Cornea* 1995;14:3-9.

80. Hahnel C, Somodi S, Slowik C, et al. Fluorescence microscopy and three-dimensional imaging of the porcine corneal keratocyte network. *Graefes Arch Clin Exp Ophthalmol* 1997;235:773-779.

81. Bourne WM. Cellular changes in transplanted human corneas. *Cornea* 2001;20:560-569.

82. Patel SV, McLaren JW, Hodge DO, Bourne WM. Keratocyte density in long term contact lens wearers. *Invest Ophthalmol Vis Sci* 2002;43:995-1003.

83. Nau CH, Erie JC, McLaren JW, et al. Keratocyte density in Fuchs' endothelial dystrophy. *Invest Ophthalmol Vis Sci* 2000;41:S270.

84. Mitooka K, Ramirez M, Maguire LJ, et al. Keratocyte density of central human corneas after laser in situ keratomileusis. *Am J Ophthalmol* 2002;103:307-314.

85. Corbett MC, Prydal JI, Verma S, et al. In vivo investigation of the structures responsible for corneal haze after photorefractive keratectomy and their effect on visual function. *Ophthalmology* 1996;103:1366-1380.

86. Fini EM. Keratocyte and fibroblast phenotypes in the repairing cornea. *Prog Ret Eye Res* 1999;18:529-551.

87. Fantes FE, Hanna KD, Waring GO, et al. Wound healing after excimer laser keratomileusis in monkeys. *Arch Ophthalmol* 1990;108:665-675.

88. Moller-Pedersen T, Cavanagh HD, Petroll WM, et al. Corneal haze development after PRK is regulated by volume of stromal tissue removal. *Cornea* 1998;17:627-639.

89. Essepian JP, Rajipal RK, Azar DT, et al. The use of confocal microscopy in evaluating corneal wound healing after excimer laser keratectomy. *Scanning* 1993;16:300-304.

90. Schimmelpfenning B. Nerve structures in human central corneal epithelium. *Graefes Arch Clin Exp Ophthalmol* 1982;218:14-20.

91. Auran JD, Koester CJ, Kleiman NJ, et al. Scanning slit confocal microscopic observation of cell morphology and movement within the normal human anterior cornea. *Ophthalmology* 1995;102:33-41.

92. Chiou AG-Y, Kaufman SC, Beuerman et al. Differential diagnosis of linear corneal images on confocal microscopy. *Cornea* 1999;18:63-66.

93. Linna TU, Vesaluoma MH, Perez-Santonja JJ, et al. Effect of myopic LASIK on corneal sensitivity and morphology of subbasal nerves. *Invest Ophthalmol Vis Sci* 2000;41:393-397.

94. Linna TU, Perez-Santonja JJ, Tervo K, et al. Recovery of corneal nerve morphology following laser in situ keratomileusis. *Exp Eye Res* 1998;66:755-763.

95. Linna T, Tervo T. Real-time confocal microscopic observations on human corneal nerves and wound healing after excimer laser photorefractive keratectomy. *Curr Eye Res* 1997;16:640-649.

96. Tervo K, Tervo TM, Eranko L, et al. Substance P-immunoreactive nerves in the human cornea and iris. *Invest Ophthalmol Vis Sci* 1982;23:671-674.

97. Tervo K, Latvala TM, Tervo TM. Recovery of corneal innervation following photorefractive keratoablation. *Arch Ophthalmol* 1994;112:1466-1470.

98. Tovainen M, Tervo T, Partanen M, et al. Histochemical demonstration of adrenergic nerves in the stroma of human cornea. *Invest Ophthalmol Vis Sci* 1987;28:398-400.

99. Ueda S, Del Cerro M, Lo Cascio JA, et al. Peptidergic and catecholaminergic fibers in the human corneal epithelium. An immunohistochemical and electron microscopic study. *Acta Ophthalmol Suppl* 1989;192:80-90.

100. Rosenberg ME, Tervo T, Immonen IJ, et al. Corneal structure and sensitivity in type I diabetes mellitus. *Invest Ophthalmol Vis Sci* 2000;41:2915-2921.

101. Lee BH, McLaren JW, Erie JC, et al. Reinnervation in the cornea after LASIK. *Invest Ophthalmol Vis Sci* 2002;43:3660-3664.

102. Slowik C, Somodi S, Thaer A, et al. Das Wundheilungsverhalten intrastromaler Hornhautlasionen nach Laser in situ Kertaomileusis. In: Rochels R, ed. 9. Kongress der DGII. Berlin: Springer; 1995:523-531.

103. Kauffmann T, Bodanowitz S, Hesse L, et al. Corneal rein-nervation after photorefractive keratectomy and laser in situ keratomileusis: an in vivo study with a confocal videomicroscope. *Ger J Ophthalmol* 1996;5:508-512.

104. Tervo TM, Linna T. Confocal microscopic findings on human corneas after PRK. *Invest Ophthalmol Vis Sci* 1996(suppl);37:71.

105. Alleman N, Chamon W, Silverman RH, et al. High-frequency ultrasound quantitative analyses of corneal scar-ring following excimer laser keratectomy. *Arch Ophthalmol* 1993;111:968-973.

106. Binder PS, Bosem M, Weinreb RN. Scheimpflug anterior segment photography assessment of wound healing after myopic excimer laser photorefractive keratectomy. *J Cataract Refract Surg* 1996;22:205-212.

107. Andrade HA, McDonald MB, Liu JC, et al. Evaluation of an opacity lensometer for determining corneal clarity following excimer laser photoablation. *Refract Corneal Surg* 1990;6:346-351.

108. Lohmann CP, Timberlake GT, Fitzke FW, et al. Corneal light scattering after excimer laser photorefractive keratec-tomy: the objective measurements of haze. *Refract Corneal Surg* 1992;8:114-121.

109. Braunstein RE, Jain S, McCally RL, et al. Objective meas-urement of corneal light scattering after excimer laser kera-tectomy. *Ophthalmology* 1996;103:439-443.

110. Moller-Pedersen T, Cavanagh HD, Petroll WM, et al. Stromal wound healing explains refractive instability and haze development after photorefractive keratectomy. *Ophthalmology* 2000;107:1235-1244.

111. Lee YG, Chen WYW, Petroll M, et al. Corneal haze after photorefractive keratectomy using different epithelial removal techniques. *Ophthalmology* 2001;108:112-120.

112. Petroll WM, Jester JV, Cavanagh HD. Quantitative three-dimensional confocal imaging of the cornea in situ and in vivo: system design and calibration. *Scanning* 1996;18:45-49.

113. Petroll WM, Jester JV, Cavanagh HD. In vivo confocal imaging: general principles and applications [review]. *Scanning* 1994;16:131-149.

114. Kim JH, Kim MS, Hahn TW, et al. Five year results of photorefractive keratectomy for myopia. *J Cataract Refract Surg* 1997;23:731-735.

115. O'Brart DPS, Corbett MC, Verma S, et al. Effects of abla-tion diameter, depth, and edge contour on the outcome of photorefractive keratectomy. *J Refract Surg* 1996;12:50-60.

116. Zieske JD, Gipson IK. Agents that affect corneal wound healing: modulation of structure and function. In: Albert DM, Jacobiec FA, eds. *Principles and Practice of Ophthalmology*. 2nd ed. Philadelphia: WB Saunders; 2000:364-372.

117. Crosson CE, Klyce SD, Beurerman RW. Epithelial wound closure in the rabbit cornea; a biphasic process. *Invest Ophthalmol Vis Sci* 1986;27:464-473.

118. Gipson IK, Kiorpes TC. Epithelial sheet movement: protein and glycoprotein synthesis. *Dev Biol* 1982;92:259-262.

119. Gipson IK, Anderson RA. Actin filaments in normal and migrating corneal epithelial cells. *Invest Ophthalmol Vis Sci* 1977;16:161-166.

120. Tuft SJ, Gartry DS, Rawe IM, et al. Photorefractive kerate-ctomy: implications of corneal wound healing. *Br J Ophthalmol* 1993;77:243-247.

121. Kuwabara T, Perkins DS, Coggan DG. Sliding of the epithelium in experimental corneal wounds. *Invest Ophthalmol Vis Sci* 1976;15:4-14.

122. Seiler T, Kahle G, Kriegerowski M, et al. Excimer laser (193 nm) myopic keratomileusis in sighted and blind human eyes. *Refract Corneal Surg* 1990;6:165-173.

123. Tuft SJ, Zabel RW, Marshall J. Corneal repair following kera-tectomy—a comparison between conventional surgery and laser ablation. *Invest Ophthalmol Vis Sci* 1989;30:1769-1777.

124. Ebata B, Friends J, Thoft R. Comparison of limbal and peripheral human corneal epithelium in tissue culture. *Invest Ophthalmol Vis Sci* 1988;29:1533-1537.

125. Cortsarelis G, Cheng S-Z, Dong G, et al. Existence of slow cycling limbal epithelial basal cells that can be preferen-tially stimulated to proliferate: implications on epithelial stem cells. *Cell* 1989;57:210-219.

126. Wilson SE, Liu JJ, Mohan RR. Stromal-epithelial interac-tions in the cornea. *Prog Retin Eye Res* 1999;18:293-309.

127. Dua HS, Gomes JAP, Singh A. Corneal epithelial wound healing. *Br J Ophthalmol* 1994;78:401-408.

128. Hanna KD, Pouliquien YM, Savoldelli M, et al. Corneal wound healing in monkeys 18 months after excimer laser photorefrac-tive keratectomy. *Refract Corneal Surg* 1990;6:340-345.

129. Fagerholm P. Wound healing after photorefractive keratec-tomy. *J Cataract Refract Surg* 2000;26:432-447.

130. Dohlman CH, Gasset AR, Rose J. The effect of the absence of corneal epithelium or endothelium on stromal kerato-cytes. *Invest Ophthalmol Vis Sci* 1968;7:520-534.

131. Nakayasu K. Stromal changes following removal of epithe-lium in rat cornea. *Jpn J Ophthalmol* 1988;32:113-125.

132. Crosson CE. Cellular changes following epithelial abrasion. In: Beuerman RW, Crosson CE, Kaufamn HE, eds. *Healing Processes in the Cornea*. Houston, Tex: Gulf Publishing Co; 1989:3-14.

133. Campos M, Szerenyi K, Lee M, et al. Keratocyte loss after corneal deepithelialization in primates and rabbits. *Arch Ophthalmol* 1994;112:254-260.

134. Bently E, Campbell S, Woo HM, et al. The effect of chronic corneal epithelial debridement on epithelial and stromal morphology in dogs. *Invest Ophthalmol Vis Sci* 2002;43:2136-2142.

135. Wilson SE, He Y-G, Weng J, et al. Epithelial injury induces keratocyte apoptosis: hypothesized role for the interleukin-1 system in the modulation of conreal tissue organization and wound healing. *Exp Eye Res* 1996;62:325-338.

136. Mohan RR, Kim WJ, Stark GR, et al. Defective keratocyte apoptosis in response to epithelial injury in stat 1 null mice. *Exp Eye Res* 2000;70:485-491.

137. Wilson SE, Kim W-J. Keratocyte apoptosis: implications on corneal wound healing, tissue organization, and disease. *Invest Ophthalmol Vis Sci* 1998;39:220-226.

138. Wilson SE, Li Q, Weng J, et al. The Fas/Fas ligand system and other modulators of apoptosis in the cornea. *Invest Ophthalmol Vis Sci* 1996;37:1582-1592.

139. Mohan RR, Liang Q, Kim W-J, et al. Apoptosis in the cornea: further characteristics of Fas-Fas ligand system. *Exp Eye Res* 1997;65:575-589.

140. Mohan RR, Kim W-J, Mohan RR, et al. Bone morphogenic proteins 2 and 4 and their receptors in the adult human cornea. *Invest Ophthalmol Vis Sci* 1998;39:2626-2636.

141. Wilson SE, Mohan RR, Hong J-H, et al. The wound healing response after laser in situ keratomileusis and photorefractive keratectomy. *Arch Ophthalmol* 2001;119:889-896.

142. Hutcheon SR, Guimaraes SR, Zieske JD. Keratocyte proliferation in response to epithelial debridment. *Invest Ophthlamol Vis Sci* 1999;40:S622

143. Zieske JD, Gimaraes SR, Hutcheon AE. Kinetics of keratocyte proliferation in response to epithelial debridement. *Exp Eye Res* 2001;72:33-39.

144. Jester JV, Huang J, Barry-Lane PA, et al. Transforming growth factor (beta)-mediated corneal myofibroblast differentiation requires actin and fibronectin assembly. *Invest Ophthlamol Vis Sci* 1999;40:1959-1967.

145. Masur SK, Dewal HS, Dinh TT, et al. Myofibroblasts differentiate from fibroblasts when plated at low density. *Proc Natl Acad Sci U S A* 1996;93:4219-4223.

146. Kim W-J, Mohan RR, Mohan RR, et al. Effect of PDGF, IL-1 alpha, and BMP2/4 on corneal fibroblast chemotaxis: expression of the platelet-derived growth factor system in the cornea. *Invest Ophthalmol Vis Sci* 1999;40:1364-1372.

147. Wilson SE. Role of apoptosis in wound healing in the cornea. *Cornea* 2000;19:S7-12.

148. Ross R, Everett NB, Tyler R. Wound healing and collagen formation. *J Cell Biol* 1970;44:645-654.

149. Garana RMR, Petroll M, Chen W-T, et al. Radial keratotomy: II. Role of the myofibroblast in corneal wound contraction. *Invest Ophthlamol Vis Sci* 1992;33:3271-3282.

150. Latvala T, Tervo K, Mustonen R, et al. Expression of cellular fibronectin and tenascin in the rabbit cornea after excimer laser photorefractive keratectomy: a twelve month study. *Br J Ophthalmol* 1995;79:65-69.

151. Cintron C, Hong B-S, Kublin CL. Quantitative analysis of collagen from normal developing corneas and corneal scars. *Curr Eye Res* 1981;1:1-7.

152. Taliana L, Evans MD, Dimitrijevich SD, et al. Vitronectin and fibronectin is required for corneal fibroblast-seeded collagen gel contraction. *Invest Ophthalmol Vis Sci* 2000;41:103-109.

153. Strissel KJ, Rinehart WB, Fini ME. Regulatin of paracrine cytokine balance controlling collagenase synthesis by corneal cells. *Invest Ophthalmol Vis Sci* 1997;38:546-552.

154. Weng J, Mohan RR, Li Q, et al. IL-1 upregulates keratinocyte growth factor and hepatocyte growth factor mRNA and protein production by cultured stromal fibroblast cells: interleukin-1 beta expression in the cornea. *Cornea* 1997;16:465-471.

155. Wilson SE, Chen L, Mohan RR, et al. Expression of HGF, KGF, EGF, and receptor messenger RNAs following corneal epithelial wounding. *Exp Eye Res* 1999;68:377-397.

156. Jester JV, Rodrigues MM, Herman IM. Characterization of avascular corneal wound healing fibroblasts: new insights into the myofibroblast. *Am J Pathol* 1987;127:140-148.

157. Jester JV, Petroll WM, Cavanagh HD. Corneal stromal wound healing in refractive surgery; the role of myofibroblasts. *Prog Ret Eye Res* 1999;18:311-356.

158. Zieske JD. Extracellular matrix and wound healing. *Curr Opin Ophthalmol* 2001;12:237-241.

159. Gao J, Gelber-Schwab TA, Addeo JV, et al. Apoptosis in the rabbit cornea after photorefractive keratectomy. *Cornea* 1997;16:200-208.

160. Wilson SE, Mohan RR, Hong JW, et al. The wound healing response after laser in situ keratomileusis and photorefractive keratectomy, elusive control of biological variability and effect on custom laser vision correction. *Arch Ophthalmol* 2001;119:889-896.

161. Helena MC, Baerveldt F, Kim WJ, et al. Keratocyte apoptosis after corneal surgery. *Invest Ophthalmol Vis Sci* 1998;39:276-283.

162. Chew S-J, Beuerman RW, Kaufman HE, et al. In vivo confocal microscopy of corneal wound healing after excimer laser photorefractive keratectomy. *CLAO* 1995;21:273-280.

163. Hanna KD, Pouliquen Y, Waring GO III, et al. Corneal stromal wound healing in rabbits after 193-nm excimer laser surface ablation. *Arch Ophthalmol* 1989;107:895-901.

164. Park CK, Kim JH. Comparison of wound healing after photorefractive keratectomy and laser in situ keratomileusis in rabbits. *J Cataract Refract Surg* 1999;25:842-850.

165. Marshall J, Trokel SL, Rothery S, et al. Longterm healing of the central cornea after photorefractive keratectomy using an excimer laser. *Ophthalmology* 1988;95:1411-1421.

166. Beuerman RW, McDonald MB, Shofner RS, et al. Quantitative histological studies of primate corneas after excimer laser photorefractive keratectomy. *Arch Ophthalmol* 1994;112:1103-1110.

167. McDonald MB, Frantz JM, Klyce SD, et al. One-year refractive results of central photorefractive keratectomy for myopia in the nonhuman primate cornea. *Arch Ophthalmol* 1990;108:40-47.

168. Malley DS, Steinert RF, Puliafito CA, et al. Immunofluorescence study of corneal wound healing after excimer laser anterior keratectomy in the monkey eye. *Arch Ophthalmol* 1990;108:1316-1322.

169. Del Pero RA, Gigstad JE, Roberts AD, et al. A refractive and histopathologic study of excimer laser keratectomy in primates. *Am J Ophthalmol* 1990;109:419-429.

170. Balestrazzi E, DeMolfetta V, Spadea L, et al. Histological, immunohistochemical, and ultrastructural findings in human corneas after photorefractive keratectomy. *J Refract Surg* 1995;11:181-187.

171. Taylor DM, L'Esperance FA Jr, Del V, et al. Human excimer laser lamellar keratectomy. A clinical study. *Ophthalmology* 1989;96:654-664.

172. Wu WC, Stark WJ, Green WR. Corneal wound healing after 193-nm excimer laser keratectomy. *Arch Ophthalmol* 1991;109:1426-1432.

173. Lohmann C, Gartry D, Kerr et al. "Haze" in photorefractive keratectomy: its origins and consequences. *Laser Light Ophthalmol* 1991;4:15-34.

174. Hersh PS, Stulting RD, Steinert F, et al. Results of phase III excimer laser photorefractive keratectomy for myopia. The Summit PRK Study Group. *Ophthalmology* 1997;104:1535-1553.

175. Gartry DS, Kerr Muir MG, Marshall J. Excimer laser photorefractive keratectomy: 18-month follow up. *Ophthalmology* 1992;99:1209-1219.

176. Seiler T, Holschbach A, Derse M, et al. Complications of myopic photorefractive keratectomy with the excimer laser. *Ophthalmology* 1994;101:153-160.

177. Kremer I, Kaplan A, Novikov I, et al. Patterns of late corneal scarring after photorefractive keratecomy in high and severe myopia. The Melbourne Excimer Laser and Research Group. *Arch Ophthalmol* 1995;113:431-436.

178. Seiler T, Kahle G, Kriegerowski M. Excimer laser (193 nm) myopic keratomileusis in sighted and blind human eyes. *Refract Corneal Surg* 1990;6:165-173.

179. Seiler T,Wollensak J. Myopic photorefractive keratectomy with the excimer laser: one-year follow-up. *Ophthalmology* 1991;98:1156-1163.

180. Chan W, Hunt KE, Glasgow BJ, et al. Corneal scarring after photorefractive keratectomy in a penetrating keratoplasty. *Am J Ophthalmol* 1996;5:570-571.

181. Binder PS, Anderson JA, Rock ME, et al. Human excimer laser keratectomy. *Ophthalmology* 1994;101:979-989.

182. L'Esperance FA Jr, Taylor DM, Marmer JW. Human excimer laser keratectomy: short-term histopathology. *J Cataract Refract Surg* 1988;4:118-124.

183. Weber B, Fagerholm P, Johansson. Colocalization of hyaluron and water in rabbit corneas after photorefractive keratectomy by specific staining for hyaluronan and by quantitative microradiography. *Cornea* 1997;16:560-563.

184. Martinez R. Etude sur l'innervation de las cornee humaine. *Invest Biol* 1940;32:75-109.

185. Beuerman RW, Kupke K. Neural regeneration following experimental wounds of the cornea in the rabbit. In: Hollyfield JG, ed. *The Structure of the Eye*. Amsterdam: Elsvier; 1982:319-330.

186. Rozsa AJ, Guss RB, Beuerman RW. Neural remodeling following experimental surgery of the rabbit cornea. *Invest Ophthalmol Vis Sci* 1983;24:1033-1051.

187. Trabucchi G, Brancato R, Verdi M, et al. Corneal nerve damage and regeneration after excimer laser photokeratomy in rabbit eyes. *Invest Ophthalmol Vis Sci* 1994;35:229-235.

188. Pallikaris I, Paptzanaki M, Georgiadis A, et al. A comparative study on neural regeneration following corneal wounds induced by argon fluoride excimer laser and mechanical methods. *Lasers Light Ophthalmol* 1990;3:89-95.

189. Ishikawa T, del Cerro M, Liang FQ, et al. Corneal sensitivity and nerve regeneration after excimer laser ablation. *Cornea* 1994;13:225-231.

190. Zeger SL, Liang KY. Longitudinal data analysis for discrete and continuous outcomes. *Biometrics* 1986;42:121-130.

191. Shieh E, Moreira H, D'Arey J, et al. Quantitative analysis of wound healing after cylindrical and spherical excimer laser ablations. *Ophthalmology* 1992;99:1050-1055.

192. Hamberg-Nystrom H, Gauthier CA, Holden, et al. A comparative study of epithelial hypertrophy after PRK: Summit versus VISX in the same patient. *Acta ophthalmol Scand* 1996;74:228-231.

193. Masters BR, Thaer AA. Real-time scanning slit confocal microscopy of the *in vivo* human cornea. *Appl Optics* 1994;33:695-701.

194. Gathier CA, Holden BA, Epstein D, et al. Factors affecting epithelial hyperplasia after photorefractive keratectomy. *J Cataract Refract Surg* 1997;23:1042-1050.

195. Gauthier CA, Epstein D, Holden BA, et al. Epithelial alterations following photorefractive keratectomy for myopia. *J Refract Surg* 1995;11:113-118.

196. Spadea L, Fasciani R, Necozione S, et al. Role of the corneal epithelium in refractive changes following laser in situ keratomileusis for high myopia. *J Refract Surg* 2000;16:133-139.

197. Lohman CP, Guell JC. Regression after LASIK for treatment of myopia: The role of the corneal epithelium. *Semin Ophthalmol* 1998;13:79-82.

198. Dillon EC, Eagle RC Jr, Laibson PR. Compensatory epithelial hyperplasia in human corneal disease. *Ophthalmic Surg* 1992;23:729-732.

199. Dierick HG, Missotten L. Is the corneal contour influenced by a tension in the superficial epithelial cells? A new hypothesis. *Refract Corneal Surg* 1992;8:54-59.

200. Liu JC, McDonald MB, Varnell R, et al. Myopic excimer laser photorefractive keratectomy: an analysis of clinical correlations. *Refract Corneal Surg* 1990;6:321-328.

201. Dutt S, Steinert RF, Raizman MB, et al. One year results of excimer laser photorefractive keratectomy for low to moderate myopia. *Arch Ophthalmol* 1994;112:1427-1436.

202. Munnerlyn CR, Koons SJ, Marshall J. Photorefractive keratectomy: a technique for laser refractive surgery. *J Cataract Refract Surg* 1988;14:46-52.

203. Davison PF, Galbavy EJ. Connective tissue remodeling in corneal and scleral wounds. *Invest Ophthalmol Vis Sci* 1986;27:1478.

204. Cionni RJ, Katakami C, Labrich JB, et al. Collagen metabolism following corneal laceration in rabbits. *Curr Eye Res* 1986;5:549-558.

205. Ambrosio R, Possin DD, Huang J, et al. Keratocyte apoptosis and proliferation in the early wound healing response to epithelial scraping injury in human corneas. *Proc Int Soc Eye Res* 2002;267:120.

206. Maumenee AE, Kornblueth W. Regeneration of corneal stromal cells I: Technique for destruction of corneal corpuscles by application of solidified (frozen) carbon dioxide. *Am J Ophthalmol* 1948;31:459.

207. Maumenee AE, Scholz RO. The histopathology of the ocular lesions produced by the sulfer and nitrogen mustards. *Bull Johns Hopkins Hosp* 1948;82:121.

208. Stulting RD, Thompson KP, Waring GO III, et al. the effect of photorefractive keratectomy on the corneal endothelium. *Ophthalmology* 1996;103:1357-1365.

209. Nishida T, Yasumoto K, Otori T, et al. The network structure of corneal fibroblasts in the rat as revealed by scanning electron microscopy. *Invest Ophthalmol Vis Sci* 1988;20:1887-1890.

210. Hasty DL, Hay ED. Freeze-fracture studies of the developing cell surface. I. The plasmalemma of the corneal fibroblast. *J Cell Biol* 1977;72:667-686.

211. Desmouliere A, Badid C, Bochaton-Piallat ML, et al. Apoptosis during wound healing, fibrocontractive diseases and vascular wall injury. *Int J Biochem Cell Biol* 1997;29:19-30.

212. Vesaluoma M, Perez-Santonja J, Petroll WM, et al. Corneal stromal changes induced by myopic LASIK. *Invest Ophthalmol Vis Sci* 2000;41:369-376.

213. Muller LJ, Pels E, Vrensen GFJM. The specific architecture of the anterior stroma accounts for maintenance of corneal curvature. *Br J Ophthalmol* 2001;85:437-443.

214. Bron A. The architecture of the corneal stroma. *Br J Ophthalmol* 2001;85:379-383. Van Horn DL, Doughman DJ, Harris JE, et al. Ultrastructure of human organ-cultured cornea. *Arch Ophthalmol* 1975;93:275-277.

215. Gan L, Hamberg-Nystrom H, Fagerholm P, et al. Cellular proliferation and leukocyte infiltration in the rabbit cornea after photorefractive keratectomy. *Acta Ophthalmol Scand* 2001;79:488-492.

216. Weimar V. Healing processes in the cornea. In: Duke-Elder S Perkins ES, eds. *The Transparency of the Cornea*. Oxford, England; Blackwell Scientific; 1960.

217. Kitano S, Goldman JN. Cytologic and histochemical changes in corneal wound repair. *Arch Ophthalmol* 1966;76:345-354.

218. Matsuda H, Smelser GK. Electron microscopy of corneal wound healing. *Exp Eye Res* 1973;16:427-442.

219. Sigano DS, Katsanevaki VJ, Pallikaris I. Correlation of subepithelial haze and refractive regression 1 month after PRK for myopia. *J Refract Surg* 1999;15:338-342.

220. Patel SV, Erie JC. Aberrant corneal nerve regeneration after LASIK. *J Cataract Refract Surg.* In press.

221. Varon SS, Bunge RP. Trophic mechanisms in the peripheral nervous system. *Annu Rev Neurosci* 1978;1:327.

222. Chan KY, Haschke RH. Action of a trophic factor from rabbit corneal epithelial culture on dissociated trigeminal neurons. *J Neurosci* 1981;1:1155.

223. Campos M, Hertzog L, Garpbus JJ, et al. Corneal sensitivity after photorefractive keratectomy. *Am J Ophthalmol* 1992;114:51-54.

224. Ishikara T, del Cerro M, Liang FQ, et al. Hypersensitivity following excimer laser ablation through the corneal epithelium. *Refract Corneal Surg* 1992;8:466-474.

225. Perez-Santonja JJ, Sakla HF, Cardona C, et al. Corneal sensitivity after photorefractive keratectomy and laser in situ keratomileusis for low myopia. *Am J Ophthalmol* 1999;127:497-504.

226. Kanellopoulos AJ, Pallikaris I, Donnenfeld ED, et al. Comparison of corneal sensation following photorefractive keratectomy and laser in situ keratomileusis. *J Cataract Refract Surg* 1997;23:34-38.

227. Murphy PJ, Corbett MC, Obrart DPS, et al. The effect of ablation type on corneal sensitivity in photorefractive keratectomy. *Invest Ophthalmol Vis Sci* 1996(suppl);37:265.

228. Belmonte C, Acosta MC, Schmelz M, et al. Measurement of corneal sensitivity to mechanical and chemical stimulation with a CO_2 esthesiometer. *Invest Ophthalmol Vis Sci* 1999;40:513-519.
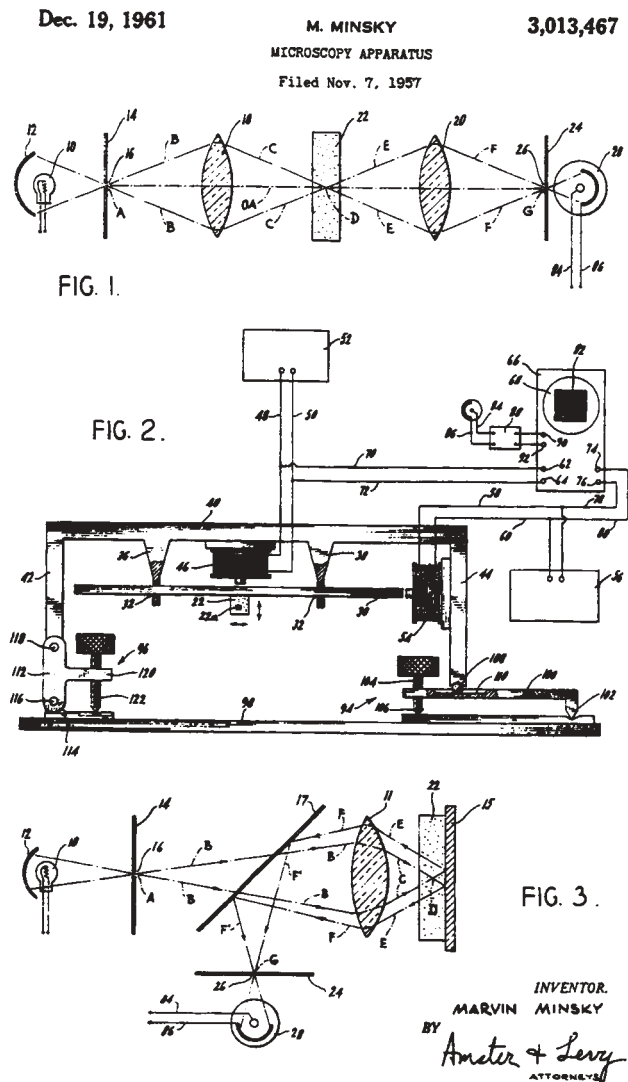
APPENDIX 1

Marvin Minsky. Microscopy apparatus. US patent 3,013,467. Dec. 19, 1961. From Masters BR. *Selected Papers on Confocal Microscopy*. Bellingham, Wash: International Society for Optical Engineering; 1996. SPIE milestone series v MS131. Reprinted with permission.
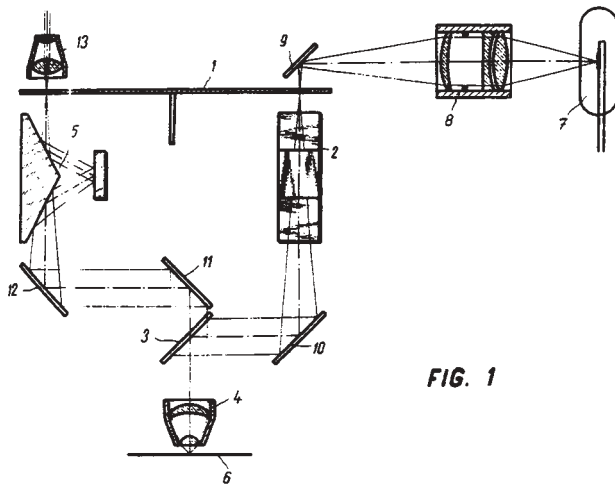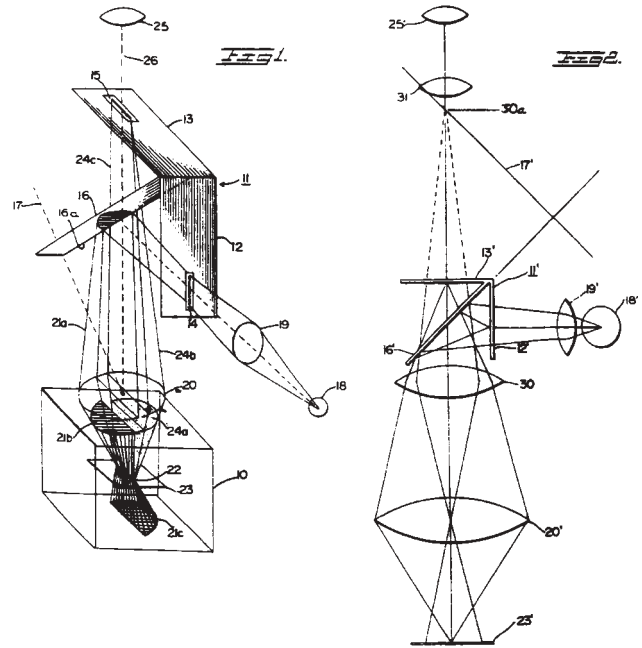
FIG. 1

APPENDIX 2
Mojmir Petran and Milan Hadravsky. Method and arrangement for improving the resolving power and contrast. US patent 3,517,980. June 30, 1970. From Masters BR. *Selected Papers on Confocal Microscopy*. Bellingham, Wash: International Society for Optical Engineering; 1996. SPIE milestone series v MS131. Reprinted with permission.

APPENDIX 3
Stephen Baer. Optical apparatus providing focal-plane-specific illumination. US patent 3,547,512. Dec 15, 1970. From Masters BR. *Selected Papers on Confocal Microscopy*. Bellingham, Wash: International Society for Optical Engineering; 1996. SPIE milestone series v MS131. Reprinted with permission.